

# Parallel Bayesian Optimization of Multiple Noisy Objectives with Expected Hypervolume Improvement

Samuel Daulton<sup>1</sup> Maximilian Balandat<sup>1</sup> Eytan Bakshy<sup>1</sup>

## Abstract

Optimizing multiple competing black-box objectives is a challenging problem in many fields, including science, engineering, and machine learning. Multi-objective Bayesian optimization is a powerful approach for identifying the optimal trade-offs between the objectives with very few function evaluations. However, existing methods tend to perform poorly when observations are corrupted by noise, as they do not take into account uncertainty in the true Pareto frontier over the previously evaluated designs. We propose a novel acquisition function, NEHVI, that overcomes this important practical limitation by applying a Bayesian treatment to the popular expected hypervolume improvement criterion to integrate over this uncertainty in the Pareto frontier. We further argue that, even in the noiseless setting, the problem of generating multiple candidates in parallel reduces that of handling uncertainty in the Pareto frontier. Through this lens, we derive a natural parallel variant of NEHVI that can efficiently generate large batches of candidates. We provide a theoretical convergence guarantee for optimizing a Monte Carlo estimator of NEHVI using exact sample-path gradients. Empirically, we show that NEHVI achieves state-of-the-art performance in noisy and large-batch environments.

## 1. Introduction

Black-box optimization problems that involve multiple competing noisy objectives are ubiquitous in science and engineering. For example, a real-time communications service may be interested in tuning the parameters of a control policy to adapt video quality in real time to maximize video quality and minimize latency (Feng et al., 2020). In robotics, scientists may seek to design hardware components that maximize locomotive speed and minimize energy expended

(Calandra et al., 2016; Liao et al., 2019). In agriculture, practitioners may seek to balance crop yield and environmental impact (Jiang et al., 2020). For such multi-objective optimization (MOO) problems, there typically is no single solution that is best with respect to all objectives. Rather, the goal is to identify the *Pareto frontier*: a set of solutions such that improving one objective means deteriorating another. In many cases, the objectives are expensive-to-evaluate and identifying the Pareto frontier with very few evaluations is imperative. For example, randomized trials used in agriculture and the internet industry may incur opportunity costs, risk, and time. Furthermore, the outcomes are often not observed precisely, but are subject to observation noise. For instance, effects of video quality are observed via A/B tests that are subject to randomization noise, sensors and actuators used in robotics are subject to uncertainties and tolerances, and agricultural trials

Bayesian optimization (BO) is a common approach for efficient, global black-box optimization. BO employs a probabilistic surrogate model and an acquisition function to navigate the trade-off between exploration (evaluating designs with high uncertainty) and exploitation (evaluating designs that are believed to be optimal).

### 1.1. Limitations of Existing Approaches

Although a significant number of works have focused on multi-objective Bayesian optimization (MOBO), most MOBO methods suffer from two practical limitations:

**Noisy observations** Much of the recent MOBO literature assumes that objectives are evaluated without noise (e.g., Yang et al. (2019c); Belakaria et al. (2019); Suzuki et al. (2020); Lukovic et al. (2020)). However, in many real-world scenarios only noisy observations of the objectives can be collected. Results of an A/B test may be highly variable due to heterogeneity in the underlying user population and other random factors. In robotics, observations of quantities such as locomotive speed and efficiency may be corrupted by measurement error from noisy sensors, manufacturing defects, and environmental factors such as temperature or surface friction. Previous work in single- and multi-objective BO have demonstrated that a principled treatment of noisy observations can significantly improve optimization perfor-

<sup>1</sup>Facebook, Menlo Park, CA, USA. Correspondence to: Samuel Daulton <sdaulton@fb.com>.

mance (Letham et al., 2019; Hernández-Lobato et al., 2014; Hernández-Lobato et al., 2015).

**Parallel candidate generation** Most MOBO methods are designed for sequential optimization and few algorithms support generating large *batches* of candidates to be evaluated in parallel, which is necessary for achieving reasonable throughput in many applications. For example, when firms optimize system parameters via A/B tests, they often do so via a large batch of candidate policies simultaneously on multiple groups of users (Letham & Bakshy, 2019) to reduce end-to-end experimentation time. In the case of microrobot design, many component designs may be fabricated in parallel on a single silicon wafer (Liao et al., 2019). And in emerging applications of Bayesian optimization like biochemistry, dozens of tests can be conducted in parallel on a single microplate (Zhang & Block, 2009).

## 1.2. Contributions

In this work, we derive a novel acquisition function, *noisy* expected hypervolume improvement (NEHVI), that employs a Bayesian treatment of observation noise by integrating over the unknown true function values at the previously evaluated points. Through this formulation, we also derive a natural parallel variant ( $q$ NEHVI) that reduces time and space complexity from exponential with respect to the batch size that  $q$  (Daulton et al., 2020) to *polynomial* in the batch size. We show how  $q$ NEHVI can be optimized effectively with gradient-based methods via sample average approximation, and demonstrate that it achieves state-of-the-art optimization performance and competitive wall times on a variety of synthetic and real-world problems.

## 2. Background

The goal in black-box optimization is to find the set of optimal designs that maximizes one or more objectives  $\mathbf{f}(\mathbf{x}) \in \mathbb{R}^M$ , with no known analytical formula nor gradient information, over a bounded set  $\mathbf{x} \in \mathcal{X} \subset \mathbb{R}^d$ .

### 2.1. Multi-Objective Optimization

In multi-objective optimization (MOO), the goal is to identify the set of Pareto optimal objective trade-offs. We say a solution  $\mathbf{f}(\mathbf{x}) = [f^{(1)}(\mathbf{x}), \dots, f^{(M)}(\mathbf{x})]$  *dominates* another solution  $\mathbf{f}(\mathbf{x}') \succ \mathbf{f}(\mathbf{x}')$  if  $f^{(m)}(\mathbf{x}) \geq f^{(m)}(\mathbf{x}')$  for  $m = 1, \dots, M$  and there exists  $m \in \{1, \dots, M\}$  such that  $f^{(m)}(\mathbf{x}) > f^{(m)}(\mathbf{x}')$ . Formally, we define the Pareto frontier (the non-dominated set) as  $\mathcal{P}^* = \{\mathbf{f}(\mathbf{x}) : \mathbf{x} \in \mathcal{X}, \nexists \mathbf{x}' \in \mathcal{X} \text{ s.t. } \mathbf{f}(\mathbf{x}') \succ \mathbf{f}(\mathbf{x})\}$ , and we denote the set of Pareto optimal designs as  $\mathcal{X}^* = \{\mathbf{x} : \mathbf{f}(\mathbf{x}) \in \mathcal{P}^*\}$ . Since the Pareto frontier is often an infinite set of points, MOO algorithms aim to identify a finite approximate Pareto fron-

tier  $\mathcal{P}$ . A natural measure of the quality of a Pareto frontier is the hypervolume dominated by the Pareto frontier and bounded from below by a reference point. Provided with the approximate Pareto frontier, the decision-maker can select an optimal solution according to their preferences.

Evolutionary algorithms (EA) such as NSGA-II (Deb et al., 2002) are popular choices for solving MOO problems (see Zitzler et al. (2000b) for a review of various other approaches). However, EAs generally suffer from high sample complexity, making them infeasible for optimizing expensive-to-evaluate black-box functions. Bayesian optimization provides a much more efficient alternative.

### 2.2. Bayesian Optimization

Bayesian optimization (BO) is a sample-efficient method that leverages a probabilistic surrogate model to make principled decisions to balance exploration and exploitation. Typically, the surrogate model is a Gaussian Process (GP): a flexible, non-parametric model known for its well-calibrated predictive uncertainty (Rasmussen, 2004). Using the surrogate model, BO employs an acquisition function  $\alpha(\mathbf{x})$  that specifies the value of evaluating a new point  $\mathbf{x}$ . Various approaches exist to quantify utility in the MOO setting, including improvement with respect to a scalarized objective (Knowles, 2006; Paria et al., 2018), improvement in the hypervolume dominated by the Pareto set (Abdolshah et al., 2018; Yang et al., 2019c), or information gain about the location of the Pareto frontier (Hernández-Lobato et al., 2015; Belakaria et al., 2019; Suzuki et al., 2020). Although evaluating the true black-box function  $\mathbf{f}$  is time-consuming, evaluating the surrogate model is relatively cheap; therefore, numerical optimization can be used to find the maximizer of the acquisition function  $\mathbf{x}^* = \arg \max_{\mathbf{x} \in \mathcal{X}_{\text{cand}}} \alpha(\mathbf{x})$  to evaluate next on the black-box function. BO sequentially selects a new point to evaluate and updates the model to incorporate the new observation. A variety of acquisition functions and heuristics are commonly used to select a batch of candidates to be evaluated on the true black-box function in parallel (Ginsbourger et al., 2010; Wang et al., 2016).

## 3. Related Work

Expected hypervolume improvement (EHVI) (Emmerich et al., 2006) is a natural extension of the popular expected improvement (EI) (Jones et al., 1998) acquisition function to the MOO setting. Recent work has led to efficient computational paradigms using box decomposition algorithms (Yang et al., 2019b) and practical enhancements such as support for parallel candidate generation and gradient-based acquisition optimization (Yang et al., 2019a; Daulton et al., 2020). However, EHVI still suffers from a few limitations including (i) the assumption that observations are noise-free, and (ii) the exponential scaling of its batch variant,

$q$ EHVI, in the batch size  $q$ , which precludes large-batch optimization.

Information-theoretic (entropy-based) methods such as PESMO (Hernández-Lobato et al., 2015), MESMO (Belakaria et al., 2019), and PFES (Suzuki et al., 2020) are an alternative to EHVI. Of these three methods, PESMO is the only one that accounts for observation noise and supports parallel evaluations (Garrido-Merchán & Hernández-Lobato, 2020). However, PESMO involves intractable entropy computations and therefore relies on difficult-to-implement approximations (Hernández-Lobato et al., 2015). Moreover, all three of the above methods involve integrating over the out-of-sample model-estimated Pareto frontier, which requires challenging and time-consuming numerical optimization of (approximate) sample draws from the GP posterior.

Thompson sampling (TS) is another popular BO strategy that is naturally robust to noise (Thompson, 1933). Paria et al. (2018) proposed using TS for MOO with random Chebyshev scalarizations (TS-TCH). However, optimizing posterior draws typically requires either (i) approximate function sampling from the GP posterior followed by numerical optimization (Rahimi & Recht, 2007) or (ii) optimization over a discrete set of candidates, which can result in sub-optimal performance even in moderately sized input spaces due to the curse of dimensionality (Pleiss et al., 2020).

Lastly, ParEGO transforms the MOO problem into a single objective problem by applying a randomly weighted augmented Chebyshev scalarization to the objectives, and maximizing the expected improvement of that scalarized quantity (Knowles, 2006). Recently, Daulton et al. (2020) used a multi-output Gaussian process and compositional Monte Carlo objective to extend ParEGO to the batch setting ( $q$ ParEGO), which proved to be a strong baseline for MOBO. Additionally, the authors proposed a noisy variant ( $q$ NParEGO), but the empirical evaluation of  $q$ NParEGO was limited.

### 3.1. Hypervolume Metrics

In this section, we review hypervolume and hypervolume improvement, as well as efficient methods for computing these metrics using box decompositions.

**Definition 1.** *The hypervolume indicator (HV) of a finite approximate Pareto frontier  $\mathcal{P}$  is the  $M$ -dimensional Lebesgue measure  $\lambda_M$  of the space dominated by  $\mathcal{P}$  and bounded from below by a reference point<sup>1</sup>  $\mathbf{r} \in \mathbb{R}^M$ :  $\text{HV}(\mathcal{P}|\mathbf{r}) = \lambda_M(\bigcup_{\mathbf{v} \in \mathcal{P}} [\mathbf{r}, \mathbf{v}])$ , where  $[\mathbf{r}, \mathbf{v}]$  denotes the hyper-rectangle bounded by vertices  $\mathbf{r}$  and  $\mathbf{v}$ .*

<sup>1</sup>As in previous work, we assume that the reference point  $\mathbf{r}$  is known and specified by the decision maker (Yang et al., 2019a).

**Definition 2.** *The hypervolume improvement (HVI) of a set of points  $\mathcal{P}'$  with respect to an existing approximate Pareto frontier  $\mathcal{P}$  and reference point  $\mathbf{r}$  is defined as:<sup>2</sup>  $\text{HVI}(\mathcal{P}'|\mathcal{P}, \mathbf{r}) = \text{HV}(\mathcal{P} \cup \mathcal{P}'|\mathbf{r}) - \text{HV}(\mathcal{P}|\mathbf{r})$ .*

Computing the hypervolume indicator requires calculating the volume of a typically non-rectangular polytope and is known to have time complexity that is super-polynomial in the number of objectives (Yang et al., 2019b). An efficient approach for computing the hypervolume is to decompose the region that is dominated by the Pareto frontier  $\mathcal{P}$  and bounded from below by a reference point  $\mathbf{r}$  into disjoint axis-aligned hyperrectangles (Lacour et al., 2017), compute the volume of each hyperrectangle in the decomposition, and sum over all hyperrectangles. So-called box decomposition algorithms have also been applied to partition the region that is *not dominated* by the Pareto frontier  $\mathcal{P}$ , which can be used to compute the hypervolume improvement from a set of new points (Dächert et al., 2017; Yang et al., 2019b). See Appendix A for further details.

### 3.2. Expected Hypervolume Improvement

Since function values at unobserved points are unknown in black-box optimization the hypervolume improvement at an out-of-sample point cannot be computed. However in the BO setting, the probabilistic surrogate model provides a posterior distribution  $p(\mathbf{f}(\mathbf{x})|\mathcal{D})$  over the function values for each  $\mathbf{x}$ , which can be used to compute the expected hypervolume improvement (EHVI) acquisition function:

$$\alpha_{\text{EHVI}}(\mathbf{x}|\mathcal{P}) = \mathbb{E}[\text{HVI}(\mathbf{f}(\mathbf{x})|\mathcal{P})]. \quad (1)$$

Although  $\alpha_{\text{EHVI}}$  can be expressed analytically when (i) the objectives are assumed to be conditionally independent given  $\mathbf{x}$ , and (ii) the candidates are generated and evaluated sequentially (Yang et al., 2019a), Monte Carlo (MC) integration is commonly used because it does not require either assumption (Emmerich et al., 2006). The MC approximation of (1) is given by

$$\alpha_{\text{EHVI}}(\mathbf{x}|\mathcal{P}) \approx \hat{\alpha}_{\text{EHVI}}(\mathbf{x}|\mathcal{P}) = \frac{1}{N} \sum_{t=1}^N \text{HVI}(\tilde{\mathbf{f}}_t(\mathbf{x})|\mathcal{P}), \quad (2)$$

where  $\tilde{\mathbf{f}}_t \sim p(\mathbf{f}|\mathcal{D})$  for  $t = 1, \dots, N$ . The same box decomposition algorithms used to compute HVI can be used to compute EHVI (either analytic or via MC) using piece-wise integration. EHVI computation is agnostic to the choice of box decomposition algorithm — even approximate methods can be employed (Couckuyt et al., 2012).

<sup>2</sup>For brevity we omit the reference point  $\mathbf{r}$  when referring to HVI.

## 4. Noisy Expected Hypervolume Improvement

To our knowledge, all previous work on EHVI assumes that observations are noiseless (Emmerich et al., 2006; Yang et al., 2019a). Instead, we consider the setting where we receive noisy observations  $\mathbf{y}_i = \mathbf{f}(\mathbf{x}_i) + \epsilon_i$ ,  $\epsilon_i \sim \mathcal{N}(0, \Sigma_i)$ , where  $\Sigma_i$  is the noise covariance. In some cases, such as when there are repeated measurements for each  $\mathbf{x}$  (e.g., for randomized experiments or stochastic simulations), we may also have access to estimates of the noise (co)variance, but the noise levels can also be inferred if such observations are unavailable.

Noisy observations pose an additional challenge because we can no longer compute the true Pareto frontier  $\mathcal{P}_n = \{\mathbf{f}(\mathbf{x}) \mid \mathbf{x} \in X_n, \nexists \mathbf{x}' \in X_n \text{ s.t. } \mathbf{f}(\mathbf{x}') \succ \mathbf{f}(\mathbf{x})\}$  over the previously evaluated points  $X_n$ . Although the posterior mean could serve as a “plug-in” estimate of the true function values at the observed points, similar heuristics for the expected improvement acquisition function in the single-objective case (Picheny et al., 2013; Gramacy et al., 2016) have been shown to suffer from poor convergence and clumped solutions due to insufficient exploration (Letham et al., 2019).

### 4.1. Noisy Expected Hypervolume Improvement

We instead take an approach similar to that in Letham et al. (2019) and derive a novel Bayesian expected hypervolume improvement acquisition function that iterates the expectation over the posterior distribution  $p(\mathcal{F}_n | \mathcal{D}_n)$  of the function values at the previously evaluated points  $\mathcal{F}_n := \mathbf{f}(X_n)$  given noisy observations  $\mathcal{D}_n = \{\mathbf{x}_i, \mathbf{y}_i, \Sigma_i\}_{i=1}^n$ . Our acquisition function, *noisy expected hypervolume improvement* (NEHVI), is defined as:

$$\alpha_{\text{NEHVI}}(\mathbf{x}) = \int \alpha_{\text{EHVI}}(\mathbf{x} | \mathcal{P}_n) p(\mathcal{F}_n | \mathcal{D}_n) d\mathcal{F}_n \quad (3)$$

Although the integral in (3) is analytically intractable, it can be approximated by MC integration. Let  $\tilde{\mathcal{F}}_t \sim p(\mathcal{F}_n | \mathcal{D}_n)$  for  $t = 1, \dots, N$  be samples from the posterior over the function values at the previously evaluated points, and let  $\mathcal{P}_t = \{\tilde{\mathbf{f}}_t(\mathbf{x}) \in \tilde{\mathcal{F}}_t \mid \tilde{\mathbf{f}}_t(\mathbf{x}) \succ \tilde{\mathbf{f}}_t(\mathbf{x}') \forall \mathbf{x}' \in X_n\}$ . Then,

$$\alpha_{\text{NEHVI}}(\mathbf{x}) \approx \frac{1}{N} \sum_{t=1}^N \alpha_{\text{EHVI}}(\mathbf{x} | \mathcal{P}_t) \quad (4)$$

Although either analytic  $\alpha_{\text{EHVI}}$  or MC-based  $\hat{\alpha}_{\text{EHVI}}$  formulations can be used to compute  $\alpha_{\text{EHVI}}$  in (4) the analytic variant requires constructing “fantasy” models, where training targets are replaced with the sampled values. Using MC integration provides a much simpler computation paradigm as the entire acquisition function can be computed using samples from the joint posterior  $\tilde{\mathbf{f}}_t(X_n, \mathbf{x}) \sim p(\mathbf{f}(X_n, \mathbf{x}) | \mathcal{D}_n)$

over  $\mathbf{x}$  and  $X_n$ :<sup>34</sup>

$$\begin{aligned} \hat{\alpha}_{\text{NEHVI}}(\mathbf{x}) &= \frac{1}{N} \sum_{t=1}^N \text{HVI}(\tilde{\mathbf{f}}_t(\mathbf{x}) | \mathcal{P}_t) \\ &= \frac{1}{N} \sum_{t=1}^N \sum_{k=1}^{K_t} \prod_{m=1}^M [z_{k,t}^{(m)} - l_{k,t}^{(m)}]_+, \end{aligned} \quad (5)$$

where  $z_{k,t}^{(m)} := \min [u_{k,t}^{(m)}, \tilde{f}_t^{(m)}(\mathbf{x})]$  and  $l_{k,t}^{(m)}, u_{k,t}^{(m)}$  are the  $m^{\text{th}}$  dimension of the lower and upper vertices of the rectangle  $S_{k,t}$  in the non-dominated partitioning  $\{S_{1,t}, \dots, S_{K_t,t}\}$  under the sampled Pareto frontier  $\mathcal{P}_t$  (see Appendix A).

## 5. Computing NEHVI

### 5.1. Cached Box Decompositions

Although  $\hat{\alpha}_{\text{NEHVI}}(\mathbf{x})$  as in (5) has a concise form, computing it requires determining the Pareto frontier  $\mathcal{P}_t$  under each sample  $\tilde{\mathbf{f}}_t$  for  $t = 1, \dots, N$  and then partitioning the region not dominated by  $\mathcal{P}_t$  into disjoint hyperrectangles  $\{S_{k,t}\}_{k=1}^{K_t}$ . Re-sampling  $\tilde{\mathbf{f}}_t$  and performing  $N$  box decompositions within each evaluation of  $\hat{\alpha}_{\text{NEHVI}}(\mathbf{x})$  during numerical optimization ( $\mathbf{x}^* = \arg \max_{\mathbf{x}} \alpha_{\text{NEHVI}}(\mathbf{x} | \mathcal{D}_n)$ ) would be prohibitively expensive because box decomposition algorithms have super-polynomial time complexity in the number of objectives (Yang et al., 2019b).

Instead, we compute the integral in (3) by fixing the samples  $\{\tilde{\mathbf{f}}_t(X_n)\}_{t=1}^N$  during the numerical optimization; this approach known as sample average approximation (SAA) (Balandat et al., 2020). Fixing the samples enables computing the Pareto frontiers and caching the box decompositions for the entirety of the acquisition function optimization, thereby making those two computationally intensive operations a one-time cost per BO iteration.<sup>5</sup> We refer to the use of these *cached box decompositions* as CBD.

### 5.2. Conditional Posterior Sampling

Under the CBD formulation, computing  $\hat{\alpha}_{\text{NEHVI}}(\mathbf{x})$  with joint samples from  $\tilde{\mathbf{f}}_t(X_n, \mathbf{x}) \sim p(\mathbf{f}(X_n, \mathbf{x}) | \mathcal{D}_n)$  requires sampling from the conditional distributions

$$\tilde{\mathbf{f}}_t(\mathbf{x}) \sim p(\mathbf{f}(\mathbf{x}) | \mathbf{f}(X_n) = \tilde{\mathbf{f}}_t(X_n), \mathcal{D}_n), \quad (6)$$

where  $t = 1, \dots, N$  and  $\{\tilde{\mathbf{f}}_t(X_n)\}_{t=1}^N$  are the realized samples at the previously evaluated points. Assuming the posterior is multivariate Gaussian (as would be the case using a GP surrogate model), we can sample from

<sup>3</sup>This “full-MC” variant also enables sampling from multi-task covariance functions across multiple correlated objectives.

<sup>4</sup>A similar joint sampling approach is used by Balandat et al. (2020) for computing integrated acquisition functions.

<sup>5</sup>For greater efficiency, we can prune  $X_n$  to remove points that are dominated with high probability, which we estimate via MC.



$p(\mathbf{f}(X_n)|\mathcal{D}_n)$  via the reparameterization trick (Kingma & Welling, 2013) by evaluating  $\tilde{\mathbf{f}}_t(\mathbf{x}) = \boldsymbol{\mu}_n + L_n^T \boldsymbol{\zeta}_{n,t}$ , where  $\boldsymbol{\zeta}_{n,t} \sim \mathcal{N}(\mathbf{0}, I_{nM})$ ,  $\boldsymbol{\mu}_n \in \mathbb{R}^{nM}$  is the posterior mean, and  $L_n \in \mathbb{R}^{nM \times nM}$  is a lower triangular root decomposition of the posterior covariance matrix, typically a Cholesky decomposition.

Given  $L_n$ , we can obtain a root decomposition  $L'_n$  of the covariance matrix of the joint posterior  $p(\mathbf{f}(X_n, \mathbf{x})|\mathcal{D}_n)$  by performing efficient low-rank updates (Osborne, 2010). Given  $L'_n$  and the posterior mean of  $p(\mathbf{f}(X_n, \mathbf{x})|\mathcal{D}_n)$ , we can sample from (6) via the reparameterization trick by augmenting the existing base samples  $\boldsymbol{\zeta}_{n,t}$  with  $M$  new base samples for the new point.

## 6. Optimizing NEHVI

### 6.1. Differentiability

Importantly,  $\hat{\alpha}_{\text{NEHVI}}(\mathbf{x})$  is differentiable w.r.t.  $\mathbf{x}$ . Although determining the Pareto frontier and computing the box decompositions are non-differentiable operations, these operations do not involve  $\mathbf{x}$ , even when re-sampling from the joint posterior  $p(\mathbf{f}(X_n, \mathbf{x})|\mathcal{D}_n)$ . Exact sample-path gradients of  $\nabla_{\mathbf{x}} \hat{\alpha}_{\text{NEHVI}}(\mathbf{x})$  can easily be computed using auto-differentiation in modern computational frameworks. This enables the use of gradient-based methods for optimizing the acquisition function, which have been shown to be crucial for efficiently optimizing EHVI-based acquisition functions (Daulton et al., 2020).<sup>6</sup>

### 6.2. SAA Convergence Results

In addition to approximating the outer expectation over  $\mathbf{f}(X_n)$  with fixed posterior samples, we can similarly fix the base samples used for the new candidate point  $\mathbf{x}$ . This approach yields a deterministic acquisition function, which enables using (quasi-) higher-order optimization methods to obtain fast convergence rates for acquisition optimization (Balandat et al., 2020). Importantly, we prove the theoretical convergence guarantees on acquisition optimization under the sample average approximation (SAA) approach proposed by Balandat et al. (2020) hold for NEHVI.

**Theorem 1.** *Suppose  $\mathcal{X}$  is compact and  $\mathbf{f}$  has a multi-output GP prior with continuously differentiable mean and covariance functions. Let  $X_n = \{\mathbf{x}_i\}_{i=1}^n$  denote the previously evaluated points and  $\{\boldsymbol{\zeta}\}_{t=1}^N$  be base samples  $\boldsymbol{\zeta} \sim \mathcal{N}(\mathbf{0}, I_{(n+1)M})$ . Let us denote the deterministic acquisition function  $\hat{\alpha}_{\text{NEHVI}}$  computed using  $\{\boldsymbol{\zeta}\}_{t=1}^N$  as  $\hat{\alpha}_{\text{NEHVI}}^N$  and define  $S^* := \arg \max_{\mathbf{x} \in \mathcal{X}} \alpha_{\text{NEHVI}}(\mathbf{x})$  to be the set of maximizers of  $\alpha_{\text{NEHVI}}(\mathbf{x})$  over  $\mathcal{X}$ . Suppose*

<sup>6</sup>One can also show that the gradient of the full MC estimator  $\hat{\alpha}_{q\text{NEHVI}}$  is an unbiased estimator of the gradient of the true joint noisy expected hypervolume improvement  $\alpha_{q\text{NEHVI}}$ . However, this result is not necessary for our SAA approach.

$\hat{\mathbf{x}}_N^* \in \arg \max_{\mathbf{x} \in \mathcal{X}} \hat{\alpha}_{\text{NEHVI}}^N(\mathbf{x})$ . Then

1.  $\hat{\alpha}_{\text{NEHVI}}^N(\hat{\mathbf{x}}_N^*) \rightarrow \alpha_{\text{NEHVI}}(\mathbf{x}_N^*)$  a.s.
2.  $\text{dist}(\hat{\mathbf{x}}_N^*, S^*) \rightarrow 0$ ,

where  $\text{dist}(\hat{\mathbf{x}}_N^*, S^*) := \inf_{\mathbf{x} \in S^*} \|\hat{\mathbf{x}}_N^* - \mathbf{x}\|$  is the Euclidean distance between  $\hat{\mathbf{x}}_N^*$  and the set  $S^*$ .

See Appendix D for further details and proof.

## 7. Parallel Noisy Expected Hypervolume Improvement

In many real-world scenarios, generating and evaluating batches of candidates is imperative to achieving adequate throughput and sufficiently fast end-to-end experimentation time. In the noiseless setting, EHVI has been extended to parallel candidate generation by considering the joint expected hypervolume improvement ( $q\text{EHVI}$ ) from a set of candidate points  $\mathcal{X}_{\text{cand}} := \{\mathbf{x}_i\}_{i=1}^q$  (Daulton et al., 2020):

$$\alpha_{q\text{EHVI}}(\mathcal{X}_{\text{cand}}|\mathcal{P}) = \int \text{HVI}(\mathbf{f}(\mathcal{X}_{\text{cand}})|\mathcal{P})p(\mathbf{f}|\mathcal{D})d\mathbf{f} \quad (7)$$

By iterating the expectation over  $p(\mathbf{f}(X_n)|\mathcal{D}_n)$ , we can write  $q\text{NEHVI}$ , as:

$$\alpha_{q\text{NEHVI}}(\mathcal{X}_{\text{cand}}) = \int \alpha_{q\text{EHVI}}(\mathcal{X}_{\text{cand}}|\mathcal{P}_n)p(\mathcal{F}_n|\mathcal{D}_n)d\mathcal{F}_n$$

Since the above integral is analytically intractable, we approximate  $q\text{NEHVI}$  using samples from the joint posterior  $p(\mathbf{f}(\mathcal{X}_{\text{cand}}, X_n)|\mathcal{D}_n)$ , similar to the sequential case:

$$\hat{\alpha}_{q\text{NEHVI}}(\mathcal{X}_{\text{cand}}) = \frac{1}{N} \sum_{t=1}^N \text{HVI}(\tilde{\mathbf{f}}_t(\mathcal{X}_{\text{cand}})|\mathcal{P}_t) \quad (8)$$

Importantly, Theorem 1 also holds in the parallel setting, so  $q\text{NEHVI}$  enjoys the same theoretical convergence guarantee as NEHVI on acquisition optimization under the SAA (see Appendix D for details).

### 7.1. Sequential Greedy Approximation

Optimizing  $q$  candidates jointly is a difficult numerical optimization problem over a  $qd$ -dimensional domain. Wilson et al. (2018) show that, in practice, many parallel MC acquisition functions can be optimized more effectively by selecting candidates sequentially in a greedy fashion. However, selecting candidates according to a “sequential greedy” policy does not guarantee that the selected batch of candidates is a maximizer of the  $\alpha_{q\text{NEHVI}}$  (it generally is not). Nevertheless, since  $q\text{NEHVI}$  is submodular, we can bound the regret of the sequential greedy approximation of  $q\text{NEHVI}$  to be no more than  $\frac{1}{e} \alpha_{q\text{NEHVI}}^*$ , where  $\alpha_{q\text{NEHVI}}^* = \max_{\mathcal{X}_{\text{cand}} \in \mathcal{X}} \alpha_{q\text{NEHVI}}$  (see Appendix E).

## 7.2. Scaling to Large Batch Sizes

Previous work on joint expected hypervolume improvement has used the inclusion-exclusion principle (IEP), which involves computing the volume jointly dominated by each of the  $2^q - 1$  nonempty subsets of points in  $\mathcal{X}_{\text{cand}}$ . Using large batch sizes is *infeasible* under IEP formulation because time and space complexity are exponential in  $q$  and multiplicative in the number of hyperrectangles in the box decomposition (Daulton et al., 2020) (see Appendix C for a complexity analysis);  $q$  must be less than 20 even under the most optimistic of circumstances.

Although the IEP can similarly be used to compute  $q$ NEHVI, we instead derive an *alternative, equivalent formulation* of  $q$ NEHVI that leverages CBD to enable scaling to large batch sizes under sequential greedy optimization.

When selecting candidate  $\mathbf{x}_i$  for  $i \in \{2, \dots, q\}$ , all candidates  $\mathbf{x}_j$  where  $j < i$  have already been selected and are therefore held constant. Thus, we can decompose  $q$ NEHVI into the  $q$ NEHVI from the previously selected candidates  $\mathbf{x}_1, \dots, \mathbf{x}_{i-1}$  and NEHVI from  $\mathbf{x}_i$ , given the previously selected candidates:

$$\begin{aligned} \hat{\alpha}_{q\text{NEHVI}}(\{\mathbf{x}_1, \dots, \mathbf{x}_i\}) \\ = \frac{1}{N} \sum_{t=1}^N \text{HVI}(\{\tilde{\mathbf{f}}_t(\mathbf{x}_j)\}_{j=1}^{i-1} \mid \mathcal{P}_t) \\ + \frac{1}{N} \sum_{t=1}^N \text{HVI}(\tilde{\mathbf{f}}_t(\mathbf{x}_i) \mid \mathcal{P}_t \cup \{\tilde{\mathbf{f}}_t(\mathbf{x}_j)\}_{j=1}^{i-1}) \end{aligned} \quad (9)$$

Note that the first term on the right hand side is constant, since  $\{\mathbf{x}_j\}_{j=1}^{i-1}$  and  $\{\tilde{\mathbf{f}}_t(\mathbf{x}_j)\}_{j=1}^{i-1}$  are fixed for all  $t = 1, \dots, N$ . The second term is  $\hat{\alpha}_{\text{NEHVI}}(\mathbf{x}_i)$ , where the NEHVI is taken with respect to the Pareto frontier across  $\mathbf{f}(X_n, \mathbf{x}_1, \dots, \mathbf{x}_{i-1})$  and computed using the fixed samples  $\{\tilde{\mathbf{f}}_t(X_n, \mathbf{x}_1, \dots, \mathbf{x}_{i-1})\}_{t=1}^N$ . To compute the second term when selecting candidate  $\mathbf{x}_i$ , the  $N$  Pareto frontiers and CBDs are updated to include  $\{\tilde{\mathbf{f}}_t(X_n, \mathbf{x}_1, \dots, \mathbf{x}_{i-1})\}_{t=1}^N$ . See appendix B.2 for derivation of (9).

Despite computing  $N$  box decompositions when selecting each candidate  $\mathbf{x}_i$  for  $i = 2, \dots, q$ , the CBD approach reduces the time and space complexity from exponential with respect to  $q$  (under the IEP) to *polynomial* with respect to  $q$ , (see Appendix C for details on time and space complexity). Figure 1 shows the total acquisition optimization time (including box decompositions) for various batch sizes and demonstrates that the CBD trick enables scaling to large batch sizes.

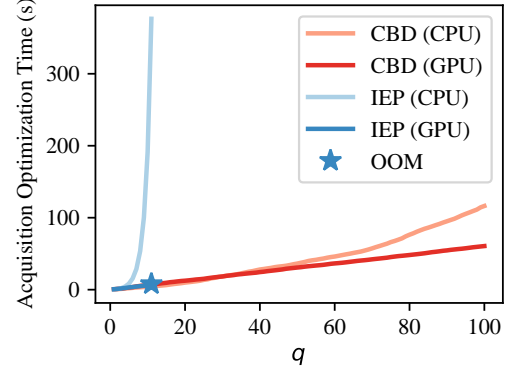


Figure 1. Acquisition optimization wall time under a sequential greedy approximation using L-BFGS-B. CBD enables scaling to much larger batch sizes  $q$  than using the inclusion-exclusion principle (IEP) and avoids running out-of-memory (OOM) on a GPU. Independent GPs are used for each outcome and are initialized with 20 points from the Pareto frontier of the 2-objective, 6-dimensional DTLZ2 problem (Deb et al., 2002). Wall times were measured on a Tesla V100 SXM2 GPU (16GB RAM) and a 2x Intel Xeon Gold 6138 CPU @ 2GHz (251GB RAM). See Appendix G.2 for results with 3 and 4 objectives.

## 8. Experiments

We empirically evaluate  $q$ NEHVI<sup>7</sup> on a set of synthetic and real-world benchmark problems. We compare it against the following recently proposed methods from the literature: MESMO<sup>7</sup> (Belakaria et al., 2019) (which we extend to the handle noisy observations using the noisy information gain from Takeno et al. (2020)), PFES<sup>7</sup> (Suzuki et al., 2020), TS-TCH<sup>8</sup> (Paria et al., 2018),  $q$ EHVI (Daulton et al., 2020) (and  $q$ EHVI-PM, which uses the posterior mean as a plug-in estimate for the function values at the in-sample points)<sup>8</sup>, and  $q$ (N)ParEGO<sup>8</sup> (Daulton et al., 2020). We optimize all methods using multi-start L-BFGS-B with exact gradients (except for PFES, which we use gradients approximated via finite differences), including TS-TCH where we optimize approximate function samples using random Fourier features (Rahimi & Recht, 2007). For  $q$ EHVI and  $q$ NEHVI, we leverage the two-step trick proposed by (Yang et al., 2019b) to perform efficient box decompositions; (i) we find the set of local lower bounds for the maximization problem using Algorithm 5 from Klamroth et al. (2015)<sup>9</sup>, and then (ii) using the local lower bounds as a Pareto frontier for the artificial minimization problem, we compute a box

<sup>7</sup>Implementations are available in the supplementary files, and will be open-sourced upon publication.

<sup>8</sup>We use the open-source implementations in BoTorch: <https://github.com/pytorch/botorch>

<sup>9</sup>More efficient methods for this step exist (e.g. Dächert et al. (2017)), but Klamroth et al. (2015) can easily leverage vectorized operations and we is sufficiently efficient in our experiments.

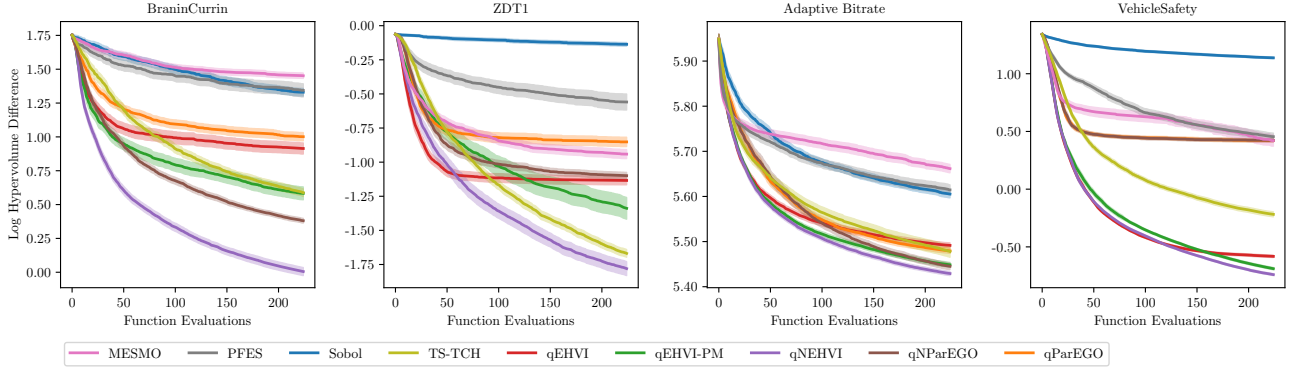


Figure 2. Sequential optimization performance. The shaded region indicates two standard errors of the mean over 100 replications.

decomposition of the dominated space using Algorithm 1 from [Lacour et al. \(2017\)](#). We model each outcome with an independent GP with a Matérn 5/2 ARD kernel and infer the GP hyperparameters via maximum a posteriori (MAP) estimation. For all problems, we assume that the noise variances are observed (except ABR, where we infer the noise level). See Appendix F for more details on the experiments.

On all problems, we evaluate all methods based on the hypervolume metric (or, equivalently, the logarithm of the difference in hypervolume between the true Pareto frontier and the approximate Pareto frontier recovered by the algorithm). Since evaluations are noisy, we compute the hypervolume dominated by the noiseless Pareto frontier across the in-sample points for each method.

**Synthetic Problems:** We consider a noisy variants of the *BraninCurrin* problem ( $M = 2, d = 2$ ) and the *ZDT1* problem ( $M = 2, d = 4$ ) ([Zitzler et al., 2000a](#)), where observations are corrupted with zero-mean additive Gaussian noise with standard deviation of 5% of the range of each objective.<sup>10</sup>

**Adaptive Bitrate (ABR) Control Policy Optimization:** Many video streaming firms adapt video bitrates during streaming to deliver the best quality of experience ([Mao et al., 2019](#)). Evaluating candidate policies typically involves running A/B tests on a subset of users to collect noisy measurements of the objectives under different policies. To minimize end-to-end optimization time, large batch sizes are often used. In this experiment, we tune a policy for ABR control to maximize video quality (bitrate) and minimize stall time. The policy has  $d = 4$  parameters, which are detailed in Appendix F. We use the Park simulator ([Mao et al., 2017](#)) and sample a random set of 100 traces to obtain noisy measurements of the objectives under a given policy. For comparing the performance of different methods, we estimate the true noiseless objective using mean objectives

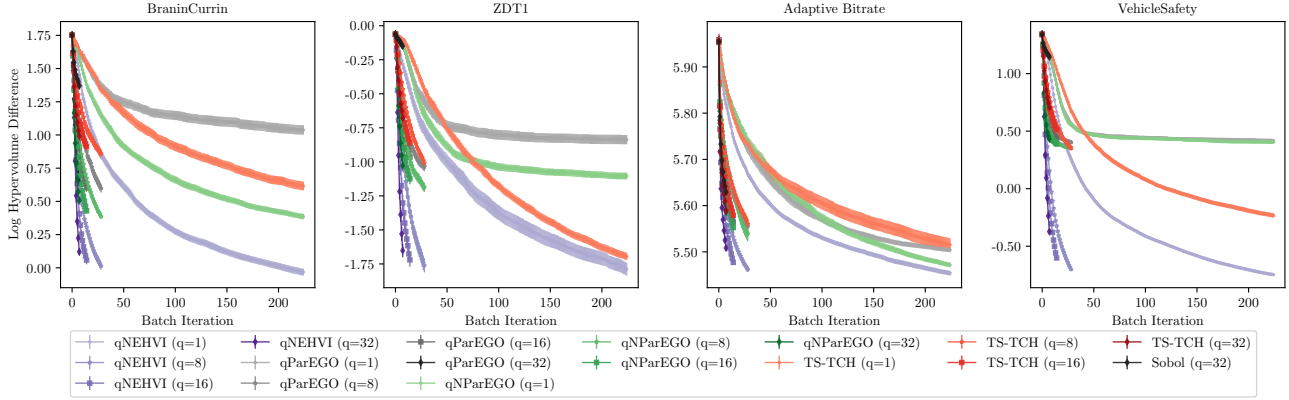
<sup>10</sup>Similar work considered a noise standard deviation of 1% of the range of each objective ([Garrido-Merchán & Hernández-Lobato, 2020](#))

across 300 traces. We infer a homoskedastic noise variance jointly with the GP hyperparameters via MAP estimation.

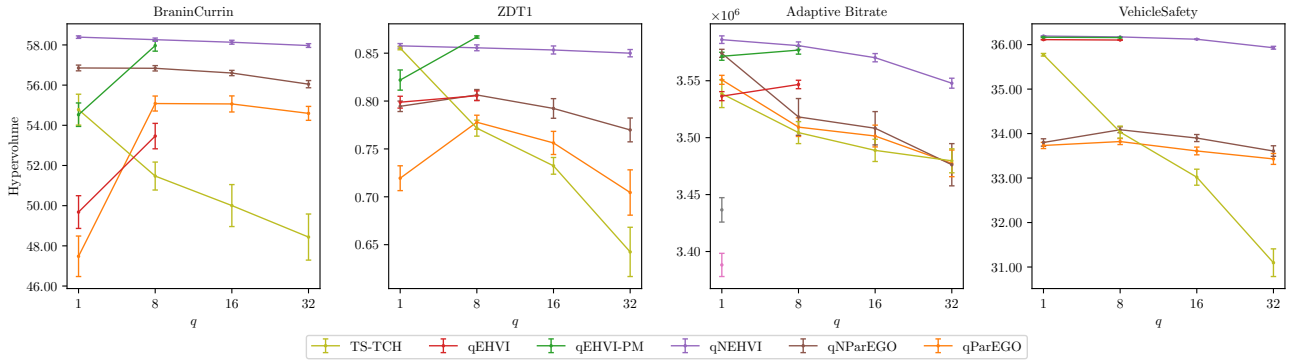
**Vehicle Design Optimization** Optimizing the design of the frame an automobile is important to maximizing passenger safety, vehicle durability and fuel efficiency. Evaluating a vehicle design is time-consuming, since either a vehicle must be manufactured and crashed, or a nonlinear finite element-based crash analysis must be run to simulate a collision (which can take over 20 hours) ([Youn et al., 2004](#)). Hence, evaluating many designs in parallel is critical for reducing end-to-end optimization time. Observations are often noisy due to manufacturing imperfections, measurement error, or non-deterministic simulations. In this experiment, we tune the width of components of a vehicle’s frame to 1) minimize mass (a proxy for fuel efficiency), 2) minimize acceleration (a proxy for passenger trauma) in a full-frontal collision, and 3) minimize the distance that the toe-board intrudes into the cabin (a proxy for vehicle fragility) ([Tanabe & Ishibuchi, 2020](#)). For this demonstration, we add zero-mean Gaussian noise with a standard deviation of 1% of the objective range, which roughly corresponds to the manufacturing noise level used in previous work ([Youn et al., 2004](#)).

## 8.1. Summary of results

We find that for  $q$ NEHVI outperforms all other methods on the noisy benchmarks, both in the sequential and parallel setting. In the sequential setting (Fig 2),  $q$ NEHVI is followed closely by  $q$ EHVI-PM, and in some cases, even  $q$ EHVI. TS-TCH is firmly in the middle of the pack, while information-theoretic acquisition functions appear to perform the most poorly. In the parallel setting (Fig 3(a)), we again find that  $q$ NEHVI provides excellent anytime performance all values of  $q$  that we tested. While parallel evaluation can provide optimization speedups on order of the batch size  $q$ , these evaluations do affect the overall sample complexity of the algorithm, since less information is available within the synchronous batch setting compared with fully sequential optimization. We find that by and large,  $q$ NEHVI achieves the greatest HV for increasingly large



(a) Optimization performance vs batch iterations



(b) Changes in sample complexity due to increased levels of parallelism

Figure 3. (a) Optimization performance of batch acquisition functions using various  $q$  over the number of BO iterations. To improve readability, we omit  $q$ EHVI(-PM) in this figure because the IEP cannot scale beyond  $q = 8$  because of the exponential time and space complexity (running it on a GPU runs out of memory and running it on a CPU results in unreasonably slow wall times). See Appendix G for results using  $q$ EHVI(-PM). (b) Quality of the final Pareto frontier identified by each method with increasing batch sizes  $q$  given a budget of 224 function evaluations.  $q$ EHVI(-PM) is only included for  $q = 1$  and  $q = 8$  because the IEP scales exponential with  $q$ .

batch sizes, and scales more elegantly relative to TS-TCH and the ParEGO variants (Fig 3(b)). We note that while  $q$ EHVI-PM tends to produce comparable performance to that of  $q$ NEHVI in the small batch regime,  $q$ EHVI(-PM) cannot scale to the large-batch regime because it relies on the IEP.

**Optimization wall time:** Across all experiments, we observe competitive wall times for optimizing  $q$ NEHVI and we provide those wall time comparisons in Appendix G. On a GPU, optimizing NEHVI is faster than optimizing than MESMO and PFES on all problems.

## 9. Discussion

We proposed  $(q)$ NEHVI, a novel acquisition function for multi-objective Bayesian optimization that by handling noisy observations and scaling to large batch sizes overcomes two core limitations of existing approaches. We demonstrated that  $(q)$ NEHVI achieves clear improvements

in optimization performance and scalability of over the state-of-the-art and that  $(q)$ NEHVI is computationally feasible for real-world BO workloads.

Yet, our work has some limitations. While the information-theoretic acquisition functions tested here perform poorly on our benchmarks, they do allow for decoupled evaluations of different objectives in cases where querying one objective may be more resource intensive than querying other objectives. Optimizing such acquisition functions is a non-trivial task, and it is possible that with improved procedures, such acquisition functions could yield improved performance and provide a principled approach to selecting evaluation sources on a budget. Further, the scalability of  $(q)$ NEHVI with respect to the number of objectives is still limited by the efficiency of box decomposition algorithms. Achieving reasonable wall times for problems with a large number of objectives may require approximate box decompositions that may reduce the effectiveness of hypervolume methods when the approximation error is substantial.



## References

- Abdolshah, M., Shilton, A., Rana, S., Gupta, S., and Venkatesh, S. Expected hypervolume improvement with constraints. In *2018 24th International Conference on Pattern Recognition (ICPR)*, pp. 3238–3243, 2018.
- Asadpour, A., Nazerzadeh, H., and Saberi, A. Stochastic submodular maximization. In Papadimitriou, C. and Zhang, S. (eds.), *Internet and Network Economics*. Springer Berlin Heidelberg, 2008.
- Balandat, M., Karrer, B., Jiang, D. R., Daulton, S., Letham, B., Wilson, A. G., and Bakshy, E. BoTorch: A Framework for Efficient Monte-Carlo Bayesian Optimization. In *Advances in Neural Information Processing Systems 33*, 2020.
- Belakaria, S., Deshwal, A., and Doppa, J. R. Max-value entropy search for multi-objective bayesian optimization. In *Advances in Neural Information Processing Systems 32*, 2019.
- Calandra, R., Seyfarth, A., Peters, J., and Deisenroth, M. P. Bayesian optimization for learning gaits under uncertainty. *Annals of Mathematics and Artificial Intelligence*, 76(1):5–23, Feb 2016. ISSN 1573-7470. doi: 10.1007/s10472-015-9463-9.
- Couckuyt, I., Deschrijver, D., and Dhaene, T. Towards efficient multiobjective optimization: Multiobjective statistical criteria. In *2012 IEEE Congress on Evolutionary Computation*, pp. 1–8, 2012.
- Daulton, S., Balandat, M., and Bakshy, E. Differentiable expected hypervolume improvement for parallel multi-objective Bayesian optimization. In *Advances in Neural Information Processing Systems 33*, NeurIPS, 2020.
- Deb, K., Pratap, A., Agarwal, S., and Meyarivan, T. A fast and elitist multiobjective genetic algorithm: Nsga-ii. *IEEE Transactions on Evolutionary Computation*, 6(2): 182–197, 2002.
- Deb, K., Thiele, L., Laumanns, M., and Zitzler, E. Scalable multi-objective optimization test problems. volume 1, pp. 825–830, 06 2002. ISBN 0-7803-7282-4. doi: 10.1109/CEC.2002.1007032.
- Deb, K., Gupta, S., Daum, D., Branke, J., Mall, A. K., and Padmanabhan, D. Reliability-based optimization using evolutionary algorithms. *IEEE Transactions on Evolutionary Computation*, 13(5):1054–1074, 2009. doi: 10.1109/TEVC.2009.2014361.
- Dächert, K., Klamroth, K., Lacour, R., and Vanderpooten, D. Efficient computation of the search region in multi-objective optimization. *European Journal of Operational Research*, 260(3):841 – 855, 2017.
- Emmerich, M. T. M., Giannakoglou, K. C., and Naujoks, B. Single- and multiobjective evolutionary optimization assisted by gaussian random field metamodells. *IEEE Transactions on Evolutionary Computation*, 10(4):421–439, 2006.
- Feng, Q., Letham, B., Bakshy, E., and Mao, H. High-Dimensional Contextual Policy Search with Unknown Context Rewards using Bayesian Optimization. In *Advances in Neural Information Processing Systems 33*, 2020.
- Fisher, M. L., Nemhauser, G. L., and Wolsey, L. A. *An analysis of approximations for maximizing submodular set functions—II*, pp. 73–87. Springer Berlin Heidelberg, Berlin, Heidelberg, 1978.
- Garrido-Merchán, E. C. and Hernández-Lobato, D. Predictive entropy search for multi-objective bayesian optimization with constraints. *Neurocomputing*, 361:50–68, 2019.
- Garrido-Merchán, E. C. and Hernández-Lobato, D. Parallel predictive entropy search for multi-objective bayesian optimization with constraints, 2020.
- Gelbart, M. A., Snoek, J., and Adams, R. P. Bayesian optimization with unknown constraints. In *Proceedings of the 30th Conference on Uncertainty in Artificial Intelligence*, UAI, 2014.
- Ginsbourger, D., Le Riche, R., and Carraro, L. *Kriging Is Well-Suited to Parallelize Optimization*, pp. 131–162. Springer Berlin Heidelberg, Berlin, Heidelberg, 2010.
- Gramacy, R. B., Gray, G. A., Digabel, S. L., Lee, H. K. H., Ranjan, P., Wells, G., and Wild, S. M. Modeling an augmented lagrangian for blackbox constrained optimization. *Technometrics*, 58(1):1–11, 2016.
- Hernández-Lobato, J. M., Hoffman, M. W., and Ghahramani, Z. Predictive entropy search for efficient global optimization of black-box functions. In *Proceedings of the 27th International Conference on Neural Information Processing Systems - Volume 1*, NIPS’14, pp. 918–926, Cambridge, MA, USA, 2014. MIT Press.
- Hernández-Lobato, D., Hernández-Lobato, J. M., Shah, A., and Adams, R. P. Predictive entropy search for multi-objective bayesian optimization, 2015.
- Jiang, S., Zhang, H., Cong, W., Liang, Z., Ren, Q., Wang, C., Zhang, F., and Jiao, X. Multi-objective optimization of smallholder apple production: Lessons from the bohai bay region. *Sustainability*, 12(16):6496, 2020.
- Jones, D. R., Schonlau, M., and Welch, W. J. Efficient global optimization of expensive black-box functions. *Journal of Global Optimization*, 13:455–492, 1998.

- Kingma, D. P. and Welling, M. Auto-Encoding Variational Bayes. *arXiv e-prints*, pp. arXiv:1312.6114, Dec 2013.
- Klamroth, K., Lacour, R., and Vanderpooten, D. On the representation of the search region in multi-objective optimization. *European Journal of Operational Research*, 245(3):767–778, Sep 2015. ISSN 0377-2217. doi: 10.1016/j.ejor.2015.03.031. URL <http://dx.doi.org/10.1016/j.ejor.2015.03.031>.
- Knowles, J. Parego: a hybrid algorithm with on-line landscape approximation for expensive multiobjective optimization problems. *IEEE Transactions on Evolutionary Computation*, 10(1):50–66, 2006.
- Lacour, R., Klamroth, K., and Fonseca, C. M. A box decomposition algorithm to compute the hypervolume indicator. *Computers & Operations Research*, 79:347 – 360, 2017.
- LeCun, Y., Cortes, C., and Burges, C. Mnist handwritten digit database. *ATT Labs [Online]*. Available: <http://yann.lecun.com/exdb/mnist>, 2, 2010.
- Letham, B. and Bakshy, E. Bayesian optimization for policy search via online-offline experimentation. *Journal of Machine Learning Research*, 20(145):1–30, 2019. URL <http://jmlr.org/papers/v20/18-225.html>.
- Letham, B., Karrer, B., Ottoni, G., and Bakshy, E. Constrained bayesian optimization with noisy experiments. *Bayesian Analysis*, 14(2):495–519, 06 2019. doi: 10.1214/18-BA1110.
- Liao, T., Wang, G., Yang, B., Lee, R., Pister, K., Levine, S., and Calandra, R. Data-efficient learning of morphology and controller for a microrobot. In *2019 International Conference on Robotics and Automation (ICRA)*, pp. 2488–2494. IEEE, 2019.
- Lukovic, K. M., Tian, Y., and Matusik, W. Diversity-guided multi-objective bayesian optimization with batch evaluations. *Advances in Neural Information Processing Systems*, 33, 2020.
- Mao, H., Netravali, R., and Alizadeh, M. Neural adaptive video streaming with pensieve. In *Proceedings of the Conference of the ACM Special Interest Group on Data Communication, SIGCOMM ’17*, pp. 197–210, New York, NY, USA, 2017. Association for Computing Machinery. ISBN 9781450346535. doi: 10.1145/3098822.3098843. URL <https://doi.org/10.1145/3098822.3098843>.
- Mao, H., Chen, S., Dimmery, D., Singh, S., Blaisdell, D., Tian, Y., Alizadeh, M., and Bakshy, E. Real-world video adaptation with reinforcement learning. 2019.
- Namkoong, H., Daulton, S., and Bakshy, E. Distilled thompson sampling: Practical and efficient thompson sampling via imitation learning, 2020.
- Osborne, M. A. Bayesian gaussian processes for sequential prediction, optimisation and quadrature. 2010.
- Paria, B., Kandasamy, K., and Póczos, B. A Flexible Multi-Objective Bayesian Optimization Approach using Random Scalarizations. *ArXiv e-prints*, May 2018.
- Paria, B., Kandasamy, K., and Póczos, B. A flexible framework for multi-objective bayesian optimization using random scalarizations, 2018.
- Picheny, V., Ginsbourger, D., Richet, Y., and Caplin, G. Quantile-based optimization of noisy computer experiments with tunable precision. *Technometrics*, 55(1):2–13, 2013. doi: 10.1080/00401706.2012.707580. URL <https://doi.org/10.1080/00401706.2012.707580>.
- Pleiss, G., Jankowiak, M., Eriksson, D., Damle, A., and Gardner, J. Fast matrix square roots with applications to gaussian processes and bayesian optimization. *Advances in Neural Information Processing Systems*, 33, 2020.
- Rahimi, A. and Recht, B. Random features for large-scale kernel machines. In *Proceedings of the 20th International Conference on Neural Information Processing Systems, NIPS’07*, pp. 1177–1184, Red Hook, NY, USA, 2007. Curran Associates Inc. ISBN 9781605603520.
- Rasmussen, C. E. *Gaussian Processes in Machine Learning*, pp. 63–71. Springer Berlin Heidelberg, Berlin, Heidelberg, 2004.
- Real, E., Aggarwal, A., Huang, Y., and Le, Q. V. Regularized evolution for image classifier architecture search. *Proceedings of the AAAI Conference on Artificial Intelligence*, 33(01):4780–4789, Jul. 2019. doi: 10.1609/aaai.v33i01.33014780. URL <https://ojs.aaai.org/index.php/AAAI/article/view/4405>.
- Schuster, M. Speech recognition for mobile devices at google. In Zhang, B.-T. and Orgun, M. A. (eds.), *PRICAI 2010: Trends in Artificial Intelligence*, pp. 8–10, Berlin, Heidelberg, 2010. Springer Berlin Heidelberg. ISBN 978-3-642-15246-7.
- Suzuki, S., Takeno, S., Tamura, T., Shitara, K., and Karasuyama, M. Multi-objective Bayesian optimization using pareto-frontier entropy. In III, H. D. and Singh, A. (eds.), *Proceedings of the 37th International Conference on Machine Learning*, volume 119 of *Proceedings of Machine Learning Research*, pp. 9279–9288. PMLR, 13–18 Jul 2020. URL <http://proceedings.mlr.press/v119/suzuki20a.html>.

- Takeo, S., Fukuoka, H., Tsukada, Y., Koyama, T., Shiga, M., Takeuchi, I., and Karasuyama, M. Multi-fidelity Bayesian optimization with max-value entropy search and its parallelization. In III, H. D. and Singh, A. (eds.), *Proceedings of the 37th International Conference on Machine Learning*, volume 119 of *Proceedings of Machine Learning Research*, pp. 9334–9345. PMLR, 13–18 Jul 2020. URL <http://proceedings.mlr.press/v119/takeno20a.html>.
- Tanabe, R. and Ishibuchi, H. An easy-to-use real-world multi-objective optimization problem suite. *Applied Soft Computing*, 89:106078, 2020. ISSN 1568-4946. doi: <https://doi.org/10.1016/j.asoc.2020.106078>.
- Thompson, W. R. On the likelihood that one unknown probability exceeds another in view of the evidence of two samples. *Biometrika*, 25(3/4):285–294, 1933.
- Wang, J., Clark, S. C., Liu, E., and Frazier, P. I. Parallel bayesian global optimization of expensive functions, 2016.
- Wang, R., Xiong, J., Ishibuchi, H., Wu, G., and Zhang, T. On the effect of reference point in moea/d for multi-objective optimization. *Applied Soft Computing*, 58:25–34, 2017. ISSN 1568-4946. doi: <https://doi.org/10.1016/j.asoc.2017.04.002>. URL <https://www.sciencedirect.com/science/article/pii/S1568494617301722>.
- Wilson, J., Hutter, F., and Deisenroth, M. Maximizing acquisition functions for bayesian optimization. In *Advances in Neural Information Processing Systems 31*, pp. 9905–9916. 2018.
- Yang, K., Emmerich, M., Deutz, A., and Bäck, T. Multi-objective bayesian global optimization using expected hypervolume improvement gradient. *Swarm and Evolutionary Computation*, 44:945 – 956, 2019a. ISSN 2210-6502. doi: <https://doi.org/10.1016/j.swevo.2018.10.007>.
- Yang, K., Emmerich, M., Deutz, A. H., and Bäck, T. Efficient computation of expected hypervolume improvement using box decomposition algorithms. *CoRR*, abs/1904.12672, 2019b.
- Yang, K., Palar, P., Emmerich, M., Shimoyama, K., and Bäck, T. A multi-point mechanism of expected hypervolume improvement for parallel multi-objective bayesian global optimization. pp. 656–663, 07 2019c. doi: 10.1145/3321707.3321784.
- Youn, B. D., Choi, K., Yang, R.-J., and Gu, L. Reliability-based design optimization for crashworthiness of vehicle side impact. *Structural and Multidisciplinary Optimization*, 26:272–283, 02 2004. doi: 10.1007/s00158-003-0345-0.
- Zhang, G. and Block, D. E. Using highly efficient nonlinear experimental design methods for optimization of lactococcus lactis fermentation in chemically defined media. *Biotechnology progress*, 25(6):1587–1597, 2009.
- Zitzler, E., Deb, K., and Thiele, L. Comparison of multiobjective evolutionary algorithms: Empirical results. *Evol. Comput.*, 8(2):173–195, June 2000a. ISSN 1063-6560. doi: 10.1162/106365600568202. URL <https://doi.org/10.1162/106365600568202>.
- Zitzler, E., Deb, K., and Thiele, L. Comparison of multiobjective evolutionary algorithms: Empirical results. *Evolutionary computation*, 8(2):173–195, 2000b.

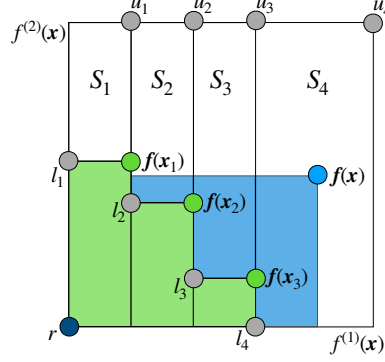


Figure 4. The hypervolume improvement from a new point  $\mathbf{f}(\mathbf{x})$  is shown in blue. The current Pareto frontier  $\mathcal{P}$  is given by the green points, the green area is the hypervolume of the Pareto frontier  $\mathcal{P}$  given reference point  $\mathbf{r}$ . The white rectangles  $S_1, \dots, S_k$  are a disjoint, box decomposition of the non-dominated space that can be used to efficiently compute the hypervolume improvement.

## A. Computing Hypervolume Improvement with Box Decompositions

**Definition 3.** For a set of objective vectors  $\{\mathbf{f}(\mathbf{x}_i)\}_{i=1}^q$ , a reference point  $\mathbf{r} \in \mathbb{R}^M$ , and a Pareto frontier  $\mathcal{P}$ , let  $\Delta(\{\mathbf{f}(\mathbf{x}_i)\}_{i=1}^q, \mathcal{P}, \mathbf{r}) \subset \mathbb{R}^M$  denote the set of points (1) that are dominated by  $\{\mathbf{f}(\mathbf{x}_i)\}_{i=1}^q$ , (2) that dominate  $\mathbf{r}$ , and (3) that are not dominated by  $\mathcal{P}$ .

Let  $\{S_1, \dots, S_K\}$  be a set of  $K$  disjoint axis-aligned rectangles where each  $S_k$  is defined by a pair of lower and upper vertices  $\mathbf{l}_k \in \mathbb{R}^M$  and  $\mathbf{u}_k \in \mathbb{R}^M \cup \{\infty\}$ . Figure 4 shows an example decomposition. Such a partitioning allows for efficient piecewise computation of the hypervolume improvement from a new point  $\mathbf{f}(\mathbf{x}_i)$  by computing the volume of the intersection of the region dominated exclusively by the new point with  $\Delta(\{\mathbf{f}(\mathbf{x}_i), \mathcal{P}, \mathbf{r})$  (and not dominated by the  $\mathcal{P}$ ) with each hyperrectangle  $S_k$ . Although  $\Delta(\{\mathbf{f}(\mathbf{x}_i), \mathcal{P}, \mathbf{r})$  is a non-rectangular polytope, the intersection of  $\Delta(\{\mathbf{f}(\mathbf{x}_i), \mathcal{P}, \mathbf{r})$  with each rectangle  $S_k$  is a rectangular polytope and the vertices bounding the hyperrectangle corresponding to  $\Delta(\{\mathbf{f}(\mathbf{x}_i), \mathcal{P}, \mathbf{r}) \cap S_k$  can be easily computed: the lower bound vertex is  $\mathbf{l}_k$  and the upper bound vertex is the component-wise minimum of  $\mathbf{u}_k$  and the new point  $\mathbf{f}(\mathbf{x})$ :  $\mathbf{z}_k := \min[\mathbf{u}_k, \mathbf{f}(\mathbf{x})]$ . The hypervolume improvement can be computed by summing over the volume of  $\Delta(\{\mathbf{f}(\mathbf{x}_i), \mathcal{P}, \mathbf{r}) \cap S_k$  over all  $S_k$

$$\text{HVI}(\mathbf{f}(\mathbf{x}), \mathcal{P}) = \sum_{k=1}^K \text{HVI}_k(\mathbf{f}(\mathbf{x}), \mathbf{l}_k, \mathbf{u}_k) = \sum_{k=1}^K \prod_{m=1}^M [z_k^{(m)} - l_k^{(m)}]_+, \quad (10)$$

where  $[\cdot]_+$  denotes the  $\max(\cdot, 0)$  operation.

## B. Derivations

### B.1. Derivation of IEP formulation of $q\text{NEHVI}$

From (8), the expected noisy joint hypervolume improvement is given by

$$\hat{\alpha}_{q\text{NEHVI}}(\mathcal{X}_{\text{cand}}) = \frac{1}{N} \sum_{t=1}^N \text{HVI}(\tilde{\mathbf{f}}_t(\mathcal{X}_{\text{cand}}) | \mathcal{P}_t)$$

Recall that the joint HVI formulation under the IEP derived by Daulton et al. (2020) is given by

$$\text{HVI}(\mathbf{f}(\mathcal{X}_{\text{cand}}) | \mathcal{P}) = \sum_{k=1}^K \sum_{j=1}^q \sum_{X_j \in \mathcal{X}_j} (-1)^{j+1} \prod_{m=1}^M [z_{k, X_j}^{(m)} - l_k^{(m)}]_+ \quad (11)$$



where  $\mathcal{X}_j := \{X_j \subseteq \mathcal{X}_{\text{cand}} : |X_j| = j\}$  and  $z_{k,t,X_j}^{(m)} := \min[u_{k,t}^{(m)}, f^{(m)}(\mathbf{x}_{i_1}), \dots, f^{(m)}(\mathbf{x}_{i_j})]$  for  $X_j = \{\mathbf{x}_{i_1}, \dots, \mathbf{x}_{i_j}\}$ . In  $q\text{NEHVI}$ , the lower and upper bounds and the number of rectangles in each box decomposition depend  $\mathcal{P}_t$ . Hence,

$$\hat{\alpha}_{q\text{NEHVI}}(\mathcal{X}_{\text{cand}}) = \frac{1}{N} \sum_{t=1}^N \sum_{k=1}^{K_t} \sum_{j=1}^q \sum_{X_j \in \mathcal{X}_j} (-1)^{j+1} \prod_{m=1}^M [z_{k,t,X_j}^{(m)} - l_{k,t}^{(m)}]_+$$

where  $z_{k,t,X_j}^{(m)} := \min[u_{k,t}^{(m)}, \tilde{f}_t^{(m)}(\mathbf{x}_{i_1}), \dots, \tilde{f}_t^{(m)}(\mathbf{x}_{i_j})]$  for  $X_j = \{\mathbf{x}_{i_1}, \dots, \mathbf{x}_{i_j}\}$ .

## B.2. Derivation of CBD formulation of $q\text{NEHVI}$

Using Definition 2, we rewrite (8) as

$$\begin{aligned} \hat{\alpha}_{q\text{NEHVI}}(\mathcal{X}_{\text{cand}}) &= \frac{1}{N} \sum_{t=1}^N \text{HVI}(\tilde{\mathbf{f}}_t(\mathcal{X}_{\text{cand}}) | \mathcal{P}_t) \\ &= \frac{1}{N} \sum_{t=1}^N \left[ \text{HV}(\tilde{\mathbf{f}}_t(\mathcal{X}_{\text{cand}}) \cup P_t) - \text{HV}(P_t) \right] \end{aligned}$$

Adding and subtracting  $\text{HV}(\tilde{\mathbf{f}}(\{\mathbf{x}_1\}, \dots, \tilde{\mathbf{f}}(x_{q-1})) \cup P_t)$  yields

$$\begin{aligned} \hat{\alpha}_{q\text{NEHVI}}(\mathcal{X}_{\text{cand}}) &= \frac{1}{N} \sum_{t=1}^N \left[ \text{HV}(\tilde{\mathbf{f}}_t(\mathcal{X}_{\text{cand}}) \cup P_t) - \text{HV}(\tilde{\mathbf{f}}(\{\mathbf{x}_1\}, \dots, \tilde{\mathbf{f}}(x_{q-1})) \cup P_t) \right. \\ &\quad \left. + \text{HV}(\{\tilde{\mathbf{f}}(\mathbf{x}_1), \dots, \tilde{\mathbf{f}}(x_{q-1})\} \cup P_t) - \text{HV}(P_t) \right]. \end{aligned}$$

Applying Definition 2 again leads to (9):

$$\hat{\alpha}_{q\text{NEHVI}}(\mathcal{X}_{\text{cand}}) = \frac{1}{N} \sum_{t=1}^N \text{HVI}(\tilde{\mathbf{f}}_t(\mathbf{x}_q) | \{\tilde{\mathbf{f}}(\mathbf{x}_1), \dots, \tilde{\mathbf{f}}(x_{q-1})\} \cup P_t) + \frac{1}{N} \sum_{t=1}^N \text{HVI}(\{\tilde{\mathbf{f}}(\mathbf{x}_1), \dots, \tilde{\mathbf{f}}(x_{q-1})\} | P_t).$$

Note that using the method of common random numbers, the CBD formulation is equivalent to IEP formulation.

## C. Complexity Analysis

### C.1. Complexity of Computing $q\text{NEHVI}$

In this section we study the complexity of computing the acquisition function. For brevity, we omit the cost of posterior sampling, which is the same for the CBD and IEP approaches.<sup>11</sup>

The CBD approach requires recomputing box decompositions when generating each new candidate. In the worst case, each new candidate is Pareto optimal under the fixed posterior samples, which leads to a time complexity of  $O(N(n+i)^M)$  for computing the box decompositions in iteration  $i$  (Yang et al., 2019b). Note that there are  $O((n+i)^M)$  rectangles in each box decomposition. Given box decompositions and posterior samples at the new point, the complexity of computing the acquisition function on a single-threaded machine is  $O(MN(n+i)^M)$ . Hence, the total time complexity for generating  $q$  candidates (ignoring potentially additional time complexity for automated gradient computations) is

$$O\left(N \sum_{i=1}^q (n+i)^M\right) + O\left(N_{\text{opt}} MN \sum_{i=1}^q (n+i)^M\right) = O(N_{\text{opt}} NM(n+q)^M q), \quad (12)$$

<sup>11</sup>Sampling from  $p(\mathbf{f}(X_n) | \mathcal{D}_n)$  incurs a one-time cost of  $O(Mn^3)$  if each of the  $M$  outcomes is modeled by an independent GP, as it involves computing a Cholesky decomposition of the  $n \times n$  posterior covariance (at the  $n$  observed points) for each. Using low-rank updates of the Cholesky factor to sample from  $p(\mathbf{f}(X_n, \mathbf{x}_0, \dots, \mathbf{x}_i) | \mathcal{D}_n)$  has a time complexity of  $O(M(n+i-1)^2)$  for  $1 \leq i \leq q$  since each triangular solve has quadratic complexity. Sampling is more costly when using a multi-task GP model, as it requires a root decomposition of the  $Mn \times Mn$  posterior covariance across data points and tasks.

$$O(Nn^M) + O\left(N_{\text{opt}}MNn^M \sum_{i=1}^q 2^{i-1}\right) = O(N_{\text{opt}}NMn^M 2^q q). \quad (13)$$

The second term on the left hand side in both (12) and (13) is the acquisition optimization complexity, which boils down to  $O(N_{\text{opt}})$  given infinite computing cores because the acquisition computation is completely parallelizable. However, as shown in Figure 1, even for relatively small values of  $q$ , CPU cores become saturated and GPU memory limits are reached.

Everything else fixed, the asymptotic relative time complexity of using CBD over IEP is therefore  $q^{-M} 2^q \rightarrow \infty$  as  $q \rightarrow \infty$ .

Similarly, the space complexity under the CBD formulation,  $O(MN(n+q)^M)$ , is also polynomial in  $q$ , whereas the space complexity is exponential in  $q$  under the IEP formulation:  $O(MNn^M q 2^q)$ .

Everything else fixed, the asymptotic relative complexity (both in terms of time and space) of using CBD over IEP is therefore  $q^M 2^{-q} \rightarrow 0$  as  $q \rightarrow \infty$ .

## C.2. Efficient Batched Computation

As noted above, using either the IEP or CBD approach, the acquisition computation given the box decompositions is highly parallelizable. However, since the number of hyperrectangles  $K_t$  in the box decomposition can be different under each posterior sample  $\mathbf{f}_t$ , stacking the box decompositions does not result in a rectangular matrix; the matrix is ragged. In order to leverage modern batched tensor computational paradigms, we pad the box decompositions with empty hyperrectangles (e.g.  $\mathbf{l} = \mathbf{0}, \mathbf{u} = \mathbf{0}$ ) such that the box decomposition under every posterior sample contains exactly  $K = \max_t K_t$  hyperrectangles, which allows us to define a  $t \times K$  dimensional matrix of box decompositions for use in batched tensor computation.

In the 2-objective case, instead of padding the box decomposition, the Pareto frontier under each posterior sample can be padded instead by repeating a point on the Pareto Frontier such that the padded Pareto frontier under every posterior sample has exactly  $\max_t |\mathcal{P}_t|$  points. This enables computing the box decompositions analytically for all posterior samples in parallel using efficient batched computation. The resulting box decompositions all have  $K = \max_t |\mathcal{P}_t| + 1$  hyperrectangles (some of which may be empty).

## D. Theoretical Results

Let  $\mathbf{x}_{\text{prev}} \in \mathbb{R}^{nd}$  denote the stacked set of previously evaluated points in  $X_n$ :  $\mathbf{x}_{\text{prev}} := [\mathbf{x}_1^T, \dots, \mathbf{x}_n^T]^T$ . Similarly, let  $\mathbf{x}_{\text{cand}} \in \mathbb{R}^{qd}$  denote the stacked set of candidates in  $\mathcal{X}_{\text{cand}}$ :  $\mathbf{x}_{\text{cand}} := [\mathbf{x}_{n+1}^T, \dots, \mathbf{x}_{n+q}^T]^T$ . Let  $\tilde{\mathbf{f}}_t(\mathbf{x}_{\text{prev}}, \mathbf{x}_{\text{cand}}) := [\tilde{\mathbf{f}}_t(\mathbf{x}_1)^T, \dots, \tilde{\mathbf{f}}_t(\mathbf{x}_{n+q})^T]^T$  denote the  $t^{\text{th}}$  sample of the corresponding objectives, which we write using the parameterization trick as

$$\tilde{\mathbf{f}}_t(\mathbf{x}_{\text{prev}}, \mathbf{x}_{\text{cand}}) = \mu(\mathbf{x}_{\text{prev}}, \mathbf{x}_{\text{cand}}) + L(\mathbf{x}_{\text{prev}}, \mathbf{x}_{\text{cand}})\boldsymbol{\zeta}_t,$$

where  $\mu(\mathbf{x}_{\text{prev}}, \mathbf{x}_{\text{cand}}) : \mathbb{R}^{(n+q)d} \rightarrow \mathbb{R}^{(n+q)M}$  is the multi-output GP's posterior mean and  $L(\mathbf{x}_{\text{cand}}, \mathbf{x}_{\text{prev}}) \in \mathbb{R}^{(n+q)M \times (n+q)M}$  is a root decomposition (often a Cholesky decomposition) of the multi-output GP's posterior covariance  $\Sigma(\mathbf{x}_{\text{cand}}, \mathbf{x}_{\text{prev}}) \in \mathbb{R}^{(n+q)M \times (n+q)M}$ , and  $\boldsymbol{\zeta}_t \in \mathbb{R}^{(n+q)M}$  with  $\boldsymbol{\zeta}_t \sim \mathcal{N}(\mathbf{0}, I_{(n+q)M})$ .<sup>12</sup>

*Proof of Theorem 1.* Since the sequential NEHVI is equivalent to the  $q$ NEHVI with  $q = 1$ , we prove Theorem 1 for the general  $q > 1$  case. Recall from Section B.2, that using the method of common random numbers to fix the base samples, the IEP and CBD formulations are equivalent. Therefore, we proceed only with the IEP formulation for this proof.

We closely follow the proof of Theorem 2 in Daulton et al. (2020). We consider the setting from Balandat et al. (2020, Section D.5). Let  $f_t^{(m)}(\mathbf{x}_i, \boldsymbol{\zeta}_t) = S_{\{i,m\}}(\mu(\mathbf{x}_{\text{cand}}, \mathbf{x}_{\text{prev}}) + L(\mathbf{x}_{\text{cand}}, \mathbf{x}_{\text{prev}})\boldsymbol{\zeta}_t)$  denote the posterior distribution over the  $m^{\text{th}}$  outcome at  $\mathbf{x}_i$  as a random variable, where  $S_{\{i,m\}}$  denotes the selection matrix ( $\|S_{\{i,m\}}\|_{\infty} \leq 1$  for all  $i = 1, \dots, n+q$  and  $m = 1, \dots, M$ ), to extract the element corresponding to outcome  $m$  for the point  $\mathbf{x}_i$ . The HVI under a single posterior sample is given by

$$A(\mathbf{x}_{\text{cand}}, \boldsymbol{\zeta}_t; \mathbf{x}_{\text{prev}}) = \sum_{k=1}^{K_t} \sum_{j=1}^q \sum_{X_j \in \mathcal{X}_j} (-1)^{j+1} \prod_{m=1}^M [z_{k,X_j}^{(m)}(\boldsymbol{\zeta}_t) - l_k^{(m)}]_+$$

<sup>12</sup>Theorem 1 can be extended to handle non-*iid* base samples from a family of quasi-Monte Carlo methods as in Balandat et al. (2020).

where  $\mathcal{X}_j := \{X_j = \{\mathbf{x}_{i_1}, \dots, \mathbf{x}_{i_j}\} \subseteq \mathcal{X}_{\text{cand}} : |X_j| = j, n+1 \leq i_1 \leq i_j \leq n+q\}$  and  $z_{k,X_j}^{(m)}(\zeta_t) = \min [u_k^{(m)}, f^{(m)}(\mathbf{x}_{i_1}, \zeta_t), \dots, f^{(m)}(\mathbf{x}_{i_j}, \zeta_t)]$ . Note that the box decomposition of the non-dominated space  $\{S_1, \dots, S_{K_t}\}$  and the number of rectangles in the box decomposition depend on  $\zeta_t$ . Importantly, the number of hyperrectangles  $K_t$  in the decomposition is a finite and bounded by  $O(|\mathcal{P}_t|^{\lfloor \frac{M}{2} \rfloor + 1})$  (Lacour et al., 2017; Yang et al., 2019b), where  $|\mathcal{P}_t| \leq n$ .

To satisfy the conditions of (Balandat et al., 2020, Theorem 3), we need to show that there exists an integrable function  $\ell : \mathbb{R}^{q \times M} \mapsto \mathbb{R}$  such that for almost every  $\zeta_t$  and all  $\mathbf{x}_{\text{cand}}, \mathbf{y}_{\text{cand}} \subseteq \mathcal{X}$ ,

$$|A(\mathbf{x}_{\text{cand}}, \zeta_t; \mathbf{x}_{\text{prev}}) - A(\mathbf{y}_{\text{cand}}, \zeta_t; \mathbf{x}_{\text{prev}})| \leq \ell(\zeta_t) \|\mathbf{x}_{\text{cand}} - \mathbf{y}_{\text{cand}}\|. \quad (14)$$

We note that  $\mathbf{x}_{\text{prev}}$  is fixed and omit  $\mathbf{x}_{\text{prev}}$  for brevity, except where necessary.

Let

$$\tilde{a}_{k,m,j,X_j}(\mathbf{x}_{\text{cand}}, \zeta_t) := \left[ \min [u_{k,t}^{(m)}, f^{(m)}(\mathbf{x}_{i_1}, \zeta_t), \dots, f^{(m)}(\mathbf{x}_{i_j}, \zeta_t)] - l_{k,t}^{(m)} \right]_+.$$

Because of linearity, it suffices to show that this condition holds for

$$\tilde{A}(\mathbf{x}_{\text{cand}}, \zeta_t) := \prod_{m=1}^M \tilde{a}_{k,m,j,X_j}(\mathbf{x}_{\text{cand}}, \zeta_t) = \prod_{m=1}^M \left[ \min [u_{k,t}^{(m)}, f^{(m)}(\mathbf{x}_{i_1}, \zeta_t), \dots, f^{(m)}(\mathbf{x}_{i_j}, \zeta_t)] - l_{k,t}^{(m)} \right]_+ \quad (15)$$

for all  $k, j$ , and  $X_j$ . Note that we can bound  $\tilde{a}_{k,m,j,X_j}(\mathbf{x}_{\text{cand}}, \zeta_t)$  by

$$\begin{aligned} \tilde{a}_{k,m,j,X_j}(\mathbf{x}_{\text{cand}}, \zeta_t) &\leq \left| \min [u_{k,t}^{(m)}, f^{(m)}(\mathbf{x}_{i_1}, \zeta_t), \dots, f^{(m)}(\mathbf{x}_{i_j}, \zeta_t)] - l_{k,t}^{(m)} \right| \\ &\leq |l_{k,t}^{(m)}| + \left| \min [u_{k,t}^{(m)}, f^{(m)}(\mathbf{x}_{i_1}, \zeta_t), \dots, f^{(m)}(\mathbf{x}_{i_j}, \zeta_t)] \right|. \end{aligned} \quad (16)$$

Consider the case where  $u_{k,t}^{(m)} = \infty$ . Then

$$\min [u_{k,t}^{(m)}, f^{(m)}(\mathbf{x}_{i_1}, \zeta_t), \dots, f^{(m)}(\mathbf{x}_{i_j}, \zeta_t)] = \min [f^{(m)}(\mathbf{x}_{i_1}, \zeta_t), \dots, f^{(m)}(\mathbf{x}_{i_j}, \zeta_t)].$$

Now suppose  $u_{k,t}^{(m)} < \infty$ . Then

$$\min [u_{k,t}^{(m)}, f^{(m)}(\mathbf{x}_{i_1}, \zeta_t), \dots, f^{(m)}(\mathbf{x}_{i_j}, \zeta_t)] < \left| \min [f^{(m)}(\mathbf{x}_{i_1}, \zeta_t), \dots, f^{(m)}(\mathbf{x}_{i_j}, \zeta_t)] \right| + |u_{k,t}^{(m)}|.$$

Let

$$w_{k,t}^{(m)} = \begin{cases} u_{k,t}^{(m)}, & \text{if } u_{k,t}^{(m)} < \infty \\ 0, & \text{otherwise.} \end{cases}$$

Note that  $l_{k,t}^{(m)}$  is finite and bounded from above and below by  $r^{(m)} \leq l_{k,t}^{(m)} < u_{k,t}^{(m)}$  for all  $k, t, m$ , where  $r^{(m)}$  is the  $m^{\text{th}}$  dimension of the reference point.

Hence, we can express the bound in (16) as

$$\begin{aligned} \tilde{a}_{k,m,j,X_j}(\mathbf{x}_{\text{cand}}, \zeta_t) &\leq |l_{k,t}^{(m)}| + |w_{k,t}^{(m)}| + \left| \min [f^{(m)}(\mathbf{x}_{i_1}, \zeta_t), \dots, f^{(m)}(\mathbf{x}_{i_j}, \zeta_t)] \right| \\ &\leq |l_{k,t}^{(m)}| + |w_{k,t}^{(m)}| + \sum_{i_1, \dots, i_j} |f^{(m)}(\mathbf{x}_{i_j}, \zeta_t)|. \end{aligned} \quad (17)$$

Note that we can bound  $\sum_{i_1, \dots, i_j} |f^{(m)}(\mathbf{x}_{i_j}, \zeta_t)|$  by

$$\sum_{i_1, \dots, i_j} |f^{(m)}(\mathbf{x}_{i_j}, \zeta_t)| \leq |X_j| (\|\mu^{(m)}(\mathbf{x}_{\text{cand}}, \mathbf{x}_{\text{prev}})\| + \|L^{(m)}(\mathbf{x}_{\text{cand}}, \mathbf{x}_{\text{prev}})\| \|\zeta_t\|).$$

Substituting this into (17) yields

$$|\tilde{a}_{k,m,j,X_j}(\mathbf{x}_{\text{cand}}, \zeta_t)| \leq |l_{k,t}^{(m)}| + |w_{k,t}^{(m)}| + |X_j| (\|\mu^{(m)}(\mathbf{x}_{\text{cand}}, \mathbf{x}_{\text{prev}})\| + \|L^{(m)}(\mathbf{x}_{\text{cand}}, \mathbf{x}_{\text{prev}})\| \|\zeta_t\|) \quad (18)$$

for all  $k, m, j, X_j$ .

Because of our assumptions of that  $\mathcal{X}$  is compact and that the mean and covariance functions are continuously differentiable,  $\mu(\mathbf{x}_{\text{cand}}, \mathbf{x}_{\text{prev}})$ ,  $L(\mathbf{x}_{\text{cand}}, \mathbf{x}_{\text{prev}})$ ,  $\nabla_{\mathbf{x}_{\text{cand}}} \mu(\mathbf{x}_{\text{cand}}, \mathbf{x}_{\text{prev}})$ , and  $\nabla_{\mathbf{x}_{\text{cand}}} L(\mathbf{x}_{\text{cand}}, \mathbf{x}_{\text{prev}})$  are uniformly bounded. Hence, there exist  $C_1, C_2 < \infty$  such that

$$|\tilde{a}_{k,m,j,X_j}(\mathbf{x}_{\text{cand}}, \zeta_t)| \leq C_1 + C_2 \|\zeta_t\|$$

for all  $k, m, j, X_j$ .

Consider the  $M = 2$  case. Omitting the indices  $k, t, j, X_j$  for brevity, we have

$$\begin{aligned} & |\tilde{A}(\mathbf{x}_{\text{cand}}, \zeta_t) - \tilde{A}(\mathbf{y}_{\text{cand}}, \zeta_t)| \\ &= |\tilde{a}_1(\mathbf{x}_{\text{cand}}, \zeta_t) \tilde{a}_2(\mathbf{x}_{\text{cand}}, \zeta_t) - \tilde{a}_1(\mathbf{y}_{\text{cand}}, \zeta_t) \tilde{a}_2(\mathbf{y}_{\text{cand}}, \zeta_t)| \\ &= |\tilde{a}_1(\mathbf{x}_{\text{cand}}, \zeta_t) (\tilde{a}_2(\mathbf{x}_{\text{cand}}, \zeta_t) - \tilde{a}_2(\mathbf{y}_{\text{cand}}, \zeta_t)) + \tilde{a}_2(\mathbf{y}_{\text{cand}}, \zeta_t) (\tilde{a}_1(\mathbf{x}_{\text{cand}}, \zeta_t) - \tilde{a}_1(\mathbf{y}_{\text{cand}}, \zeta_t))| \\ &\leq |\tilde{a}_1(\mathbf{x}_{\text{cand}}, \zeta_t)| |\tilde{a}_2(\mathbf{x}_{\text{cand}}, \zeta_t) - \tilde{a}_2(\mathbf{y}_{\text{cand}}, \zeta_t)| + |\tilde{a}_2(\mathbf{y}_{\text{cand}}, \zeta_t)| |\tilde{a}_1(\mathbf{x}_{\text{cand}}, \zeta_t) - \tilde{a}_1(\mathbf{y}_{\text{cand}}, \zeta_t)|. \end{aligned} \quad (19)$$

Using (18), we can bound  $|\tilde{a}_{k,m,j,X_j}(\mathbf{x}_{\text{cand}}, \zeta_t) - \tilde{a}_{k,m,j,X_j}(\mathbf{y}_{\text{cand}}, \zeta_t)|$  by

$$\begin{aligned} & |\tilde{a}_{k,t,m,j,X_j}(\mathbf{x}_{\text{cand}}, \zeta_t) - \tilde{a}_{k,t,m,j,X_j}(\mathbf{y}_{\text{cand}}, \zeta_t)| \\ &\leq \sum_{i_1, \dots, i_j} |S_{\{i_j, m\}}(\mu(\mathbf{x}_{\text{cand}}, \mathbf{x}_{\text{prev}}) + L(\mathbf{x}_{\text{cand}}, \mathbf{x}_{\text{prev}})\zeta_t) - S_{\{i_j, m\}}(\mu(\mathbf{y}_{\text{cand}}, \mathbf{x}_{\text{prev}}) + L(\mathbf{y}_{\text{cand}}, \mathbf{x}_{\text{prev}})\zeta_t)| \\ &\leq |X_j| \left( \|\mu(\mathbf{x}_{\text{cand}}, \mathbf{x}_{\text{prev}}) - \mu(\mathbf{y}_{\text{cand}}, \mathbf{x}_{\text{prev}})\| + \|L(\mathbf{x}_{\text{cand}}, \mathbf{x}_{\text{prev}}) - L(\mathbf{y}_{\text{cand}}, \mathbf{x}_{\text{prev}})\| \|\zeta_t\| \right). \end{aligned}$$

Since  $\mu$  and  $L$  have uniformly bounded gradients with respect to  $\mathbf{x}_{\text{cand}}$  and  $\mathbf{y}_{\text{cand}}$ , they are Lipschitz. Therefore, there exist  $C_3, C_4 < \infty$  such that

$$|\tilde{a}_{k,t,m,j,X_j}(\mathbf{x}_{\text{cand}}, \zeta_t) - \tilde{a}_{k,t,m,j,X_j}(\mathbf{y}_{\text{cand}}, \zeta_t)| \leq (C_3 + C_4 \|\zeta_t\|) \|\mathbf{x}_{\text{cand}} - \mathbf{y}_{\text{cand}}\| \quad (20)$$

for all  $\mathbf{x}_{\text{cand}}, \mathbf{y}_{\text{cand}}, k, t, m, j, X_j$ .

Substituting (20) into (19), we have

$$|\tilde{A}(\mathbf{x}_{\text{cand}}, \zeta_t) - \tilde{A}(\mathbf{y}_{\text{cand}}, \zeta_t)| \leq 2 \left( C_1 C_3 + (C_1 C_4 + C_2 C_3) \|\zeta_t\| + C_2 C_4 \|\zeta_t\|^2 \right) \|\mathbf{x}_{\text{cand}} - \mathbf{y}_{\text{cand}}\|$$

The  $M > 2$  is very similar to the  $M = 2$  case in (19) albeit with more complex expansions. Similarly, There exist  $C < \infty$  such that

$$|\tilde{A}(\mathbf{x}_{\text{cand}}, \zeta_t) - \tilde{A}(\mathbf{y}_{\text{cand}}, \zeta_t)| \leq C \sum_{m=1}^M \|\zeta_t\|^m \|\mathbf{x}_{\text{cand}} - \mathbf{y}_{\text{cand}}\|$$

Let us define  $\ell(\zeta_t) := C \sum_{m=1}^M \|\zeta_t\|^m$ . Note that  $\ell(\zeta_t)$  is integrable because all absolute moments exist for the Gaussian distribution. Since this satisfies the criteria for Theorem 3 in Balandat et al. (2020), the theorem holds for  $q\text{NEHVI}$ .  $\square$

### D.1. Unbiased Gradient estimates from the MC formulation

As noted in Section 6, we can show the following (note that this result is not actually required for Theorem 1):

**Proposition 1.** *Suppose that the GP mean and covariance function are continuously differentiable. Suppose further that the candidate set  $\mathcal{X}_{\text{cand}}$  has no duplicates, and that the sample-level gradients  $\nabla_{\mathbf{x}} \text{HVI}(\tilde{f}_t(\mathbf{x}))$  are obtained using the reparameterization trick as in Balandat et al. (2020). Then*

$$\mathbb{E}[\nabla_{\mathbf{x}_{\text{cand}}} \hat{\alpha}_{q\text{NEHVI}}^N(\mathbf{x}_{\text{cand}})] = \nabla_{\mathbf{x}_{\text{cand}}} \alpha_{q\text{NEHVI}}(\mathbf{x}_{\text{cand}}), \quad (21)$$

that is, the averaged sample-level gradient is an unbiased estimate of the gradient of the true acquisition function.

The proof of Proposition 1 closely follows the proof of Proposition 1 in Daulton et al. (2020).



## E. Error Bound on Sequential Greedy Approximation for NEHVI

If the acquisition function  $\mathcal{L}(\mathcal{X}_{\text{cand}})$  is a normalized (meaning  $\mathcal{L}(\emptyset) = 0$ ), monotone, submodular (meaning that *the increase* in  $\mathcal{L}(\mathcal{X}_{\text{cand}})$  is non-increasing as elements are added to  $\mathcal{X}_{\text{cand}}$  set function), then the sequential greedy approximation  $\hat{\mathcal{L}}$  of  $\mathcal{L}$  enjoys regret of no more than  $\frac{1}{e}\mathcal{L}^*$ , where  $\mathcal{L}^* = \max_{\mathcal{X}_{\text{cand}} \subseteq \mathcal{X}} \mathcal{L}(\mathcal{X}_{\text{cand}})$  is the optima of  $\mathcal{L}$  (Fisher et al., 1978). We have  $\alpha_{q\text{NEHVI}}(\mathcal{X}_{\text{cand}}) = \mathcal{L}(\mathcal{X}_{\text{cand}}) = \mathbb{E}_{\mathcal{P}}[\alpha_{q\text{EHVI}}(\mathcal{X}_{\text{cand}}|\mathcal{P})]$ . For a fixed, known  $\mathcal{P}$ , Daulton et al. (2020) showed that  $\alpha_{q\text{EHVI}}$  is submodular set function. In  $\alpha_{q\text{NEHVI}}$ ,  $\mathcal{P}$  is a stochastic, so  $\alpha_{q\text{EHVI}}(\mathcal{X}_{\text{cand}}|\mathcal{P})$  is a stochastic submodular set function. Because the expectation of a stochastic submodular function is submodular (Asadpour et al., 2008),  $\alpha_{q\text{NEHVI}}$  is also submodular. Hence, the sequential greedy approximation of  $\alpha_{q\text{NEHVI}}$  enjoys regret of no more than  $\frac{1}{e}\alpha_{q\text{NEHVI}}^*$ . Using the result from Wilson et al. (2018), the MC-based approximation  $\hat{\alpha}_{q\text{NEHVI}}(\mathcal{X}_{\text{cand}}) = \sum_{t=1}^N \text{HVI}[f_t(\mathcal{X}_{\text{cand}})|P_t]$  also enjoys the same regret bound because HVI is a normalized submodular set function.<sup>13</sup>

## F. Experiment Setup

### F.1. Algorithm Details

All methods are initialized with  $2(d+1)$  points from a scrambled Sobol sequence. All MC acquisition functions uses  $N = 128$  quasi-MC samples (Balandat et al., 2020). All parallel algorithms using sequential greedy optimization for selecting a batch of candidates points and the base samples are redrawn when selecting candidate  $x_i, i = 1, \dots, q$ . For PFES and MESMO, we use 10 sampled (approximate) functions using random Fourier features and optimize each function using 5000 iterations of NSGA-II (Deb et al., 2002) with a population size of 50. For PFES, we partition the dominated space under each sampled Pareto frontier using the algorithm proposed Lacour et al. (2017), which is more efficient and yields fewer hyperrectangles than the Quick Hypervolume algorithm used by the PFES authors (Suzuki et al., 2020). For  $q\text{NParEGO}$ , we use a similar pruning strategy to that in  $q\text{NEHVI}$  to only integrate over the function values of in-sample points that have positive probability of being best with respect to the sampled scalarization. We use the off-the-shelf implementation of  $q\text{NParEGO}$  in BoTorch (Balandat et al., 2020), which does not use low-rank Cholesky updates; however, we do note that  $q\text{NPAREGO}$  would likely achieve lower wall times using more efficient linear algebra tricks.

### F.2. Problem Details

All benchmark problems are treated as maximization problems; the objectives for minimization problems are multiplied by -1 to obtain an equivalent maximization problem.

**BraninCurrin** ( $M = 2, d = 2$ ) The BraninCurrin problem involves optimizing two competing functions used in BO benchmarks: Branin and Currin. The goal is minimize both:

$$\begin{aligned} f^{(1)}(x'_1, x'_2) &= (x_2 - \frac{5.1}{4\pi^2}x_1^2 + \frac{5}{\pi}x_1 - r)^2 + 10(1 - \frac{1}{8\pi})\cos(x_1) + 10 \\ f^{(2)}(x_1, x_2) &= \left[1 - \exp\left(-\frac{1}{(2x_2)}\right)\right] \frac{2300x_1^3 + 1900x_1^2 + 2092x_1 + 60}{100x_1^3 + 500x_1^2 + 4x_1 + 20} \end{aligned}$$

where  $x_1, x_2 \in [0, 1]$ ,  $x'_1 = 15x_1 - 5$ , and  $x'_2 = 15x_2$ .

**ZDT1** ( $M = 2, d = 4$ ) ZDT1 is a benchmark problem from the multi-objective optimization literature (Zitzler et al., 2000a). The goal is minimize the following two objectives

$$\begin{aligned} f^{(1)}(\mathbf{x}) &= x_1 \\ f^{(2)}(\mathbf{x}) &= g(\mathbf{x}) \left(1 - \sqrt{\frac{f^{(1)}(\mathbf{x})}{g(\mathbf{x})}}\right) \end{aligned}$$

where  $g(\mathbf{x}) = 1 + \frac{9}{d-1} \sum_{i=2}^d x_i$  and  $\mathbf{x} = [x_1, \dots, x_d] \in [0, 1]^d$ .

<sup>13</sup>Submodularity technically requires a finite search space  $\mathcal{X}$ , whereas in BO  $\mathcal{X}$  is typically an infinite set. Nevertheless in similar scenarios, submodularity has been extended to infinite sets (e.g. Wilson et al. (2018)).

PARAMETER	SEARCH SPACE
LEARNING RATE ( $\log_{10}$ SCALE)	$[-5.0, -1.0]$
LEARNING RATE DECAY MULTIPLIER	$[0.01, 1.0]$
DROPOUT RATE	$[0.0, 0.7]$
$L_1$ REGULARIZATION	$[10^{-5}, 0.1]$
$L_2$ REGULARIZATION	$[10^{-5}, 0.1]$
HIDDEN LAYER 1 SIZE	$[20, 500]$
HIDDEN LAYER 2 SIZE	$[20, 500]$
HIDDEN LAYER 3 SIZE	$[20, 500]$

Table 1. The search space for the AutoML benchmark.

**VehicleSafety** ( $M = 3$ ,  $d = 5$ ) The 3 objectives are based on a response surface model that is fit to data collected from a simulator and are given by (Tanabe & Ishibuchi, 2020):

$$\begin{aligned}
 f_1(\mathbf{x}) &= 1640.2823 + 2.3573285x_1 + 2.3220035x_2 + 4.5688768x_3 + 7.7213633x_4 + 4.4559504x_5 \\
 f_2(\mathbf{x}) &= 6.5856 + 1.15x_1 - 1.0427x_2 + 0.9738x_3 + 0.8364x_4 - 0.3695x_1x_4 + 0.0861x_1x_5 \\
 &\quad + 0.3628x_2x_4 + 0.1106x_1^2 - 0.3437x_3^2 + 0.1764x_4^2 \\
 f_3(\mathbf{x}) &= -0.0551 + 0.0181x_1 + 0.1024x_2 + 0.0421x_3 - 0.0073x_1x_2 + 0.024x_2x_3 - 0.0118x_2x_4 \\
 &\quad - 0.0204x_3x_4 - 0.008x_3x_5 - 0.0241x_2^2 + 0.0109x_4^2
 \end{aligned}$$

where  $\mathbf{x} \in [1, 3]^5$ .

**AutoML** ( $M = 2$ ,  $d = 8$ ) This experiment considers optimizing predictive performance and latency of a deep neural networks (DNN). Practitioners and researchers across many domains use DNNs for recommendation and recognition tasks in low-latency (e.g. on-device) environments (Schuster, 2010), where any increase in prediction time degrades the product experience (Namkoong et al., 2020). Simultaneously, researchers are considering increasingly larger architectures that improve predictive performance (Real et al., 2019). Therefore, a firm may be interesting understanding the set of optimal trade-offs between prediction latency and predictive performance. For a demonstration, we consider optimizing ( $d = 8$ ) hyperparameters of DNN (detailed in Table 1) to minimize out-of-sample prediction error and minimize latency on the MNIST data set (LeCun et al., 2010). Using a small randomized test set leads to noisy evaluations of predictive performance and latency measurements are often noisy due to unrelated fluctuations in the testing environment. As in previous works, we minimize a logit transformation of the prediction error and minimize a logarithm of the ratio between the latency of a proposed DNN and the latency of the fastest DNN (Hernández-Lobato et al., 2015; Garrido-Merchán & Hernández-Lobato, 2019; 2020). For each evaluation, we randomly partition the 60,000 examples from the MNIST training set into a set of 50,000 examples for training and 10,000 examples for evaluation. We train each network for 8 epochs using SGD with momentum with mini-batches of 512 examples. The learning rate is decayed after every 30 mini-batch updates using the specified decay multiplier. We use randomized rounding on the integer parameters before evaluation. For evaluating the performance of different BO methods, we estimate the noiseless objectives using the mean objectives across 3 replications. DNNs are implemented in PyTorch using ReLU activations and a softmax output layer. Latency measurements are taken on a CPU (2x Intel Xeon E5-2680 v4 @ 2.40GHz).

**CarSideImpact** ( $M = 4$ ,  $d = 7$ ) A side-impact test is common practice under European Enhanced Vehicle-Safety Committee to uphold vehicle safety standards (Deb et al., 2009). In contrast with the previous VehicleSafety problem where we considered a full-frontal collision, we now consider the problem of tuning parameters controlling the structural design of an automobile in the case of a *side-impact* collision. This problem has been widely used in various works and has previously used stochastic parameters to account for manufacturing error (Deb et al., 2009). We use the recent 4-objective version proposed by Tanabe & Ishibuchi (2020) where the goal to minimize the weight of the vehicle, passenger trauma (pubic force), and vehicle damage (the average velocity of the V-pillar). The fourth objective is a combination of 10 other measures of the vehicle durability and passenger safety (see (Deb et al., 2009) for details). The mathematical formulas for a response surface model fit to data collected from a simulator are given below:

$$\begin{aligned}
 f^{(1)}(\mathbf{x}) &= 1.98 + 4.9x_1 + 6.67x_2 + 6.98x_3 + 4.01x_4 + 1.78x_5 + 10^{-5}x_6 + 2.73x_7 \\
 f^{(2)}(\mathbf{x}) &= 4.72 - 0.5x_4 - 0.19x_2x_3 \\
 f^{(3)}(\mathbf{x}) &= 0.5(V_{\text{MBP}}(\mathbf{x}) + V_{\text{FD}}(\mathbf{x})) \\
 f^{(4)}(\mathbf{x}) &= -\sum_{i=1}^{10} \max[g_i(\mathbf{x}), 0]
 \end{aligned}$$

where

$$\begin{aligned}
 g_1(\mathbf{x}) &= 1 - 1.16 + 0.3717x_2x_4 + 0.0092928x_3 \\
 g_2(\mathbf{x}) &= 0.32 - 0.261 + 0.0159x_1x_2 + 0.06486x_1 + 0.019x_2x_7 - 0.0144x_3x_5 - 0.0154464x_6 \\
 g_3(\mathbf{x}) &= 0.32 - 0.214 - 0.00817x_5 + 0.045195x_1 + 0.0135168x_1 - 0.03099x_2x_6 \\
 &\quad + 0.018x_2x_7 - 0.007176x_3 - 0.023232x_3 + 0.00364x_5x_6 + 0.018x_2^2 \\
 g_4(\mathbf{x}) &= 0.32 - 0.74 + 0.61x_2 + 0.031296x_3 + 0.031872x_7 - 0.227x_2^2 \\
 g_5(\mathbf{x}) &= 32 - 28.98 - 3.818x_3 + 4.2x_1x_2 - 1.27296x_6 + 2.68065x_7 \\
 g_6(\mathbf{x}) &= 32 - 33.86 - 2.95x_3 + 5.057x_1x_2 + 3.795x_2 + 3.4431x_7 - 1.45728 \\
 g_7(\mathbf{x}) &= 32 - 46.36 + 9.9x_2 + 4.4505x_1 \\
 g_8(\mathbf{x}) &= 4 - f_2(\mathbf{x}) \\
 g_9(\mathbf{x}) &= 9.9 - V_{\text{MBP}}(\mathbf{x}) \\
 g_{10}(\mathbf{x}) &= 15.7 - V_{\text{FD}}(\mathbf{x}) \\
 V_{\text{MBP}}(\mathbf{x}) &= 10.58 - 0.674x_1x_2 - 0.67275x_2 \\
 V_{\text{FD}}(\mathbf{x}) &= 16.45 - 0.489x_3x_7 - 0.843x_5x_6
 \end{aligned}$$

. The search space is:

$$\begin{aligned}
 x_1 &\in [0.5, 1.5] \\
 x_2 &\in [0.45, 1.35] \\
 x_3, x_4 &\in [0.5, 1.5] \\
 x_5 &\in [0.875, 2.625] \\
 x_6, x_7 &\in [0.4, 1.2].
 \end{aligned}$$

As in the VehicleSafety problem, we add zero-mean Gaussian noise to each objective with a standard deviation of 1% the range of each objective.

**Constrained BraninCurrin ( $M = 2$ ,  $V = 2$ ,  $d = 2$ )** The constrained BraninCurrin problem uses the same objectives as BraninCurrin, but adds the following disk constraint from (Gelbart et al., 2014):

$$c(x'_1, x'_2) = 50 - (x'_1 - 2.5)^2 - (x'_2 - 7.5)^2 \geq 0$$

We add zero-mean Gaussian noise to objectives and the constraint slack observations with a standard deviation of 5% of the range of each outcome.

### F.3. Evaluation Details

To compute the log hypervolume difference metric, we use NSGA-II to estimate the true Pareto frontier (except for the ABR and AutoML problems, where evaluations are time-consuming and we instead take the true Pareto frontier to be the Pareto frontier across the estimated objectives across all methods and replications). Using this Pareto frontier, we compute the hypervolume dominated by the true Pareto frontier in order to calculate the log hypervolume difference. For ZDT1, the hypervolume dominated by the true Pareto frontier can be computed analytically. For Constrained BraninCurrin, we

PROBLEM	REFERENCE POINT
BRANINCURRIN	[-18.00, -6.00]
ZDT1	[-1.10, -1.10]
VEHICLESAFETY	[-1698.55, -11.21, -0.29]
ABR	[150.00, -3500.00]
AUTOML	[-2.45, 0.60]
CARSIDEIMPACT	[45.49, 4.51, 13.34, 10.39]
CONSTRAINEDBRANINCURRIN	[80.0, 12.0]

Table 2. The reference points for each benchmark problem.

evaluate the logarithm of the difference between the hypervolume dominated by the true feasible Pareto frontier and the feasible in-sample Pareto frontier for each method.

For all problems, we selected the reference point based on the component-wise noiseless nadir point  $\mathbf{f}_{\text{nadir}}(\mathbf{x}) = \min_{\mathbf{x} \in \mathcal{X}} \mathbf{f}(\mathbf{x})$  and the range of the Pareto frontier for each noiseless objective using the common heuristic (Wang et al., 2017):  $\mathbf{r} = \mathbf{f}_{\text{nadir}}(\mathbf{x}) - \beta * (\mathbf{f}_{\text{ideal}}(\mathbf{x}) - \mathbf{f}_{\text{nadir}}(\mathbf{x}))$ , where  $\beta = 0.1$  and  $\mathbf{f}_{\text{ideal}}(\mathbf{x}) = \max_{\mathbf{x} \in \mathcal{X}} \mathbf{f}(\mathbf{x})$ .

## G. Experiments

### G.1. Wall Time Results

Table 4 reports the acquisition optimization wall times for each method. On all benchmark problems except CarSideImpact,  $q\text{NEHVI}$  is faster to optimize than MESMO and PFES on a GPU. The wall times for optimizing  $q\text{NEHVI}$  are competitive with those for  $q\text{NParEGO}$  on most benchmark problems and batch sizes; on many problems,  $q\text{NEHVI}$  is often faster than  $q\text{NParEGO}$ . On the problems VehicleSafety and CarSideImpact problems which have 3 and 4 objectives respectively, we observed tractable wall times, even when generating  $q = 32$  candidates. The wall time for 3 and 4 objective problems is larger primarily because the box decompositions are more time-consuming to compute and result in more hyperrectangles as the number of objectives increases. Although,  $q\text{EHVI}(\text{PM})$  is faster for  $q = 1$  and  $q = 8$  on many problems, it is unable to scale to large batch sizes and ran out of memory for  $q = 8$  on CarSideImpact due to the box decomposition having a large number of hyperrectangles.



CPU	BRANINCURRIN	ZDT1	ABR	VEHICLESAFETY
MESMO ( $q=1$ )	21.24 ( $\pm 0.02$ )	19.76 ( $\pm 0.03$ )	23.24 ( $\pm 0.04$ )	28.39 ( $\pm 0.07$ )
PFES ( $q=1$ )	22.86 ( $\pm 0.05$ )	39.82 ( $\pm 0.14$ )	43.03 ( $\pm 0.12$ )	53.16 ( $\pm 0.17$ )
TS-TCH ( $q=1$ )	0.51 ( $\pm 0.0$ )	0.48 ( $\pm 0.0$ )	0.75 ( $\pm 0.0$ )	0.67 ( $\pm 0.0$ )
$q$ EHVI-PM ( $q=1$ )	2.34 ( $\pm 0.02$ )	3.7 ( $\pm 0.02$ )	3.56 ( $\pm 0.03$ )	7.82 ( $\pm 0.05$ )
$q$ EHVI ( $q=1$ )	0.58 ( $\pm 0.0$ )	0.66 ( $\pm 0.01$ )	2.98 ( $\pm 0.02$ )	5.07 ( $\pm 0.03$ )
$q$ NEHVI ( $q=1$ )	40.55 ( $\pm 0.61$ )	35.66 ( $\pm 0.47$ )	62.29 ( $\pm 0.97$ )	120.43 ( $\pm 1.25$ )
$q$ NPAREGO ( $q=1$ )	3.19 ( $\pm 0.05$ )	1.65 ( $\pm 0.02$ )	6.94 ( $\pm 0.06$ )	1.05 ( $\pm 0.01$ )
$q$ PAREGO ( $q=1$ )	0.58 ( $\pm 0.01$ )	0.7 ( $\pm 0.01$ )	2.5 ( $\pm 0.03$ )	0.75 ( $\pm 0.01$ )
GPU	BRANINCURRIN	ZDT1	ABR	VEHICLESAFETY
MESMO ( $q=1$ )	19.9 ( $\pm 0.04$ )	19.92 ( $\pm 0.04$ )	21.54 ( $\pm 0.08$ )	24.57 ( $\pm 0.09$ )
PFES ( $q=1$ )	21.68 ( $\pm 0.07$ )	45.9 ( $\pm 0.17$ )	43.3 ( $\pm 0.13$ )	47.25 ( $\pm 0.16$ )
TS-TCH ( $q=1$ )	0.88 ( $\pm 0.01$ )	0.94 ( $\pm 0.01$ )	1.08 ( $\pm 0.01$ )	1.04 ( $\pm 0.01$ )
TS-TCH ( $q=8$ )	1.85 ( $\pm 0.03$ )	2.01 ( $\pm 0.03$ )	2.99 ( $\pm 0.04$ )	2.32 ( $\pm 0.05$ )
TS-TCH ( $q=16$ )	3.08 ( $\pm 0.08$ )	3.29 ( $\pm 0.1$ )	4.28 ( $\pm 0.08$ )	3.54 ( $\pm 0.09$ )
TS-TCH ( $q=32$ )	5.25 ( $\pm 0.15$ )	5.41 ( $\pm 0.16$ )	7.23 ( $\pm 0.2$ )	6.41 ( $\pm 0.23$ )
$q$ EHVI-PM ( $q=1$ )	2.86 ( $\pm 0.02$ )	4.67 ( $\pm 0.03$ )	3.66 ( $\pm 0.03$ )	5.66 ( $\pm 0.04$ )
$q$ EHVI-PM ( $q=8$ )	68.46 ( $\pm 2.75$ )	61.47 ( $\pm 0.84$ )	41.46 ( $\pm 0.61$ )	105.67 ( $\pm 2.09$ )
$q$ EHVI ( $q=1$ )	0.72 ( $\pm 0.01$ )	0.99 ( $\pm 0.02$ )	3.67 ( $\pm 0.02$ )	3.96 ( $\pm 0.05$ )
$q$ EHVI ( $q=8$ )	18.12 ( $\pm 1.03$ )	18.05 ( $\pm 0.86$ )	40.55 ( $\pm 0.58$ )	71.49 ( $\pm 2.04$ )
$q$ NEHVI ( $q=1$ )	6.15 ( $\pm 0.06$ )	5.75 ( $\pm 0.04$ )	7.72 ( $\pm 0.09$ )	20.81 ( $\pm 0.11$ )
$q$ NEHVI ( $q=8$ )	48.19 ( $\pm 1.2$ )	46.74 ( $\pm 0.83$ )	49.7 ( $\pm 0.79$ )	168.63 ( $\pm 2.49$ )
$q$ NEHVI ( $q=16$ )	102.87 ( $\pm 4.02$ )	95.6 ( $\pm 2.62$ )	93.14 ( $\pm 1.72$ )	289.02 ( $\pm 5.82$ )
$q$ NEHVI ( $q=32$ )	177.56 ( $\pm 7.81$ )	190.59 ( $\pm 6.07$ )	181.97 ( $\pm 4.77$ )	546.83 ( $\pm 16.09$ )
$q$ NPAREGO ( $q=1$ )	2.39 ( $\pm 0.04$ )	1.84 ( $\pm 0.04$ )	6.47 ( $\pm 0.05$ )	0.9 ( $\pm 0.02$ )
$q$ NPAREGO ( $q=8$ )	47.05 ( $\pm 1.74$ )	52.99 ( $\pm 1.94$ )	74.72 ( $\pm 1.9$ )	45.56 ( $\pm 1.17$ )
$q$ NPAREGO ( $q=16$ )	118.73 ( $\pm 5.53$ )	116.68 ( $\pm 5.51$ )	116.79 ( $\pm 3.19$ )	91.3 ( $\pm 3.83$ )
$q$ NPAREGO ( $q=32$ )	306.17 ( $\pm 17.81$ )	279.01 ( $\pm 17.72$ )	240.56 ( $\pm 6.44$ )	188.42 ( $\pm 13.42$ )
$q$ PAREGO ( $q=1$ )	0.81 ( $\pm 0.02$ )	1.05 ( $\pm 0.03$ )	4.39 ( $\pm 0.05$ )	0.79 ( $\pm 0.02$ )
$q$ PAREGO ( $q=8$ )	13.01 ( $\pm 0.53$ )	16.4 ( $\pm 0.72$ )	31.02 ( $\pm 0.81$ )	12.64 ( $\pm 0.84$ )
$q$ PAREGO ( $q=16$ )	34.34 ( $\pm 2.12$ )	43.66 ( $\pm 3.12$ )	66.85 ( $\pm 3.13$ )	36.68 ( $\pm 4.48$ )
$q$ PAREGO ( $q=32$ )	139.73 ( $\pm 25.22$ )	108.25 ( $\pm 6.94$ )	122.37 ( $\pm 6.12$ )	107.34 ( $\pm 14.76$ )

Table 3. Acquisition function optimization wall time (including box decompositions) in seconds on a CPU (2x Intel Xeon E5-2680 v4 @ 2.40GHz) and a Tesla V100 SXM2 GPU (16GB RAM). The mean and two standard errors are reported.

## G.2. Scaling to large batch sizes with CBD

In Figure 5, we provide results demonstrating the CBD approach enables scaling to large batch sizes, even with 3 or 4 objectives, whereas the IEP wall times grow exponentially with the batch size and the IEP overflows GPU memory even with modest batch sizes.

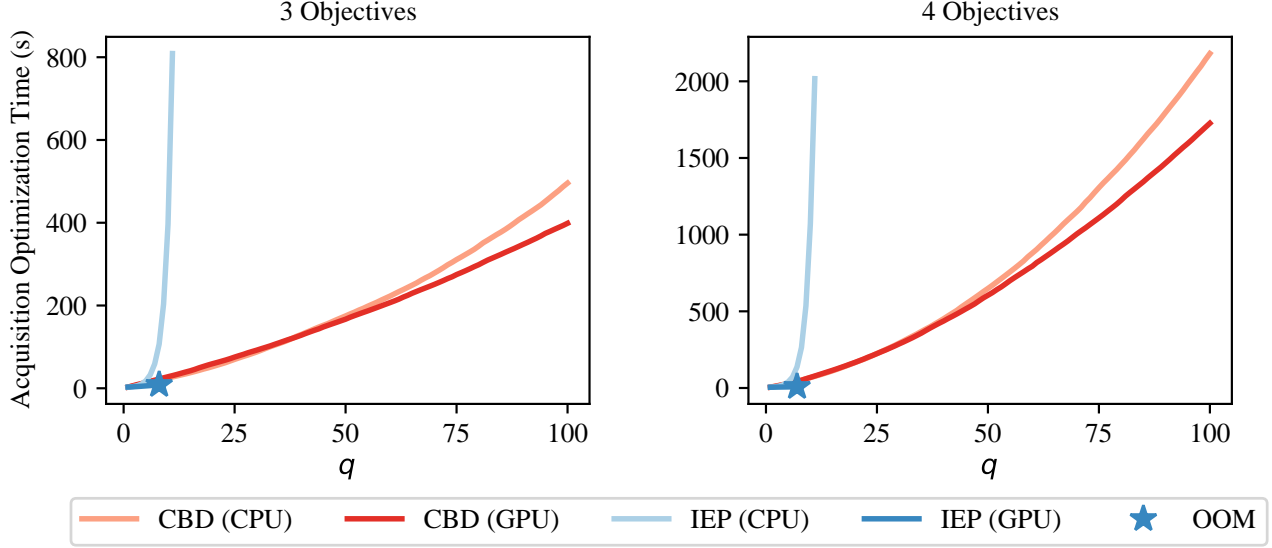


Figure 5. . Acquisition optimization wall time under a sequential greedy approximation using L-BFGS-B. CBD enables scaling to much larger batch sizes  $q$  than using the inclusion-exclusion principle (IEP) and avoids running out-of-memory (OOM) on a GPU. Independent GPs are used for each outcome and are initialized with 20 points from the Pareto frontier of the 6-dimensional DTLZ2 problem (Deb et al., 2002) with 3 objectives (left) and 4 objectives (right). Wall times were measured on a Tesla V100 SXM2 GPU (16GB GPU RAM) and a Intel Xeon Gold 6138 CPU @ 2GHz CPU (251GB RAM).

## G.3. Additional Empirical Results

The additional optimization performance results in the appendix demonstrate that  $q$ NEHVI is consistently the top performer. The only case where  $q$ NEHVI is outperformed is in the sequential setting on the CarSideImpact problem in Figure 6(a), where  $q$ EHVI performs best. However, as show in Figure 6(b) and Figure 6(c),  $q$ NEHVI enables scaling to large batch sizes, whereas  $q$ EHVI runs out of memory on a GPU for  $q = 8$ . Therefore, in a practical setting where vehicles are manufactured and test in parallel,  $q$ NEHVI would be the best choice.

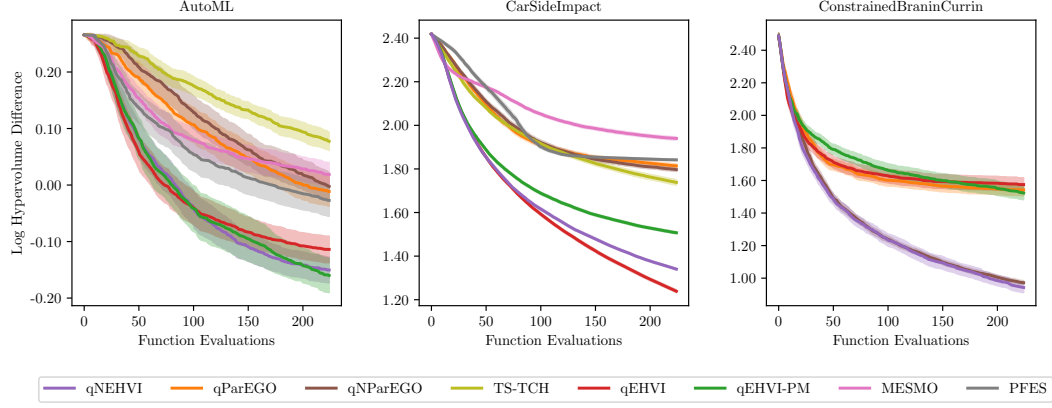
Figure 8 shows that  $q$ NEHVI achieves solid performance anytime throughout the learning curve, and Figure 9 shows that  $q$ NEHVI consistently achieves the best performance for various  $q$  with a fixed budget of 224 function evaluations.

## G.4. Better performance from $q$ EHVI with a larger batch size

In many test problems  $q$ EHVI performs better with  $q = 8$  than  $q = 1$ . In the case of BraninCurrin and Constrained-BraninCurrin,  $q$ ParEGO also improves as  $q$  increases. Since this phenomenon is not observed with the noisy acquisition functions ( $q$ NEHVI,  $q$ NParEGO), we hypothesize that it may be the case that sequential data collection results in a difficult to optimize acquisition surface and that integrating over the in-sample points leads to a smoother acquisition surface that results in improved sequential optimization. The acquisition functions that do not account for noise may be misled by the noise in sequential setting, but using a larger batch size (within limits) may help avoid the issue of not properly accounting for noise.

CPU	AUTOML	CARSideIMPACT	CONSTRAINED BRANINCURRIN
MESMO ( $q=1$ )	37.86 ( $\pm 0.08$ )	33.31 ( $\pm 0.06$ )	NA
PFES ( $q=1$ )	101.24 ( $\pm 0.29$ )	102.55 ( $\pm 0.34$ )	NA
TS-TCH ( $q=1$ )	0.93 ( $\pm 0.0$ )	1.27 ( $\pm 0.01$ )	NA
$q$ EHVI-PM ( $q=1$ )	5.76 ( $\pm 0.05$ )	83.14 ( $\pm 0.74$ )	10.27 ( $\pm 0.06$ )
$q$ EHVI ( $q=1$ )	5.05 ( $\pm 0.04$ )	96.19 ( $\pm 0.9$ )	3.26 ( $\pm 0.05$ )
$q$ NEHVI ( $q=1$ )	22.71 ( $\pm 0.48$ )	541.13 ( $\pm 6.83$ )	267.67 ( $\pm 4.09$ )
$q$ NPAREGO ( $q=1$ )	5.6 ( $\pm 0.07$ )	3.38 ( $\pm 0.05$ )	12.05 ( $\pm 0.17$ )
$q$ PAREGO ( $q=1$ )	3.06 ( $\pm 0.03$ )	1.91 ( $\pm 0.02$ )	1.56 ( $\pm 0.03$ )
GPU	AUTOML	CARSideIMPACT	CONSTRAINED BRANINCURRIN
MESMO ( $q=1$ )	28.83 ( $\pm 0.2$ )	26.0 ( $\pm 0.06$ )	NA
PFES ( $q=1$ )	85.73 ( $\pm 0.4$ )	55.41 ( $\pm 0.16$ )	NA
TS-TCH ( $q=1$ )	1.49 ( $\pm 0.01$ )	2.17 ( $\pm 0.01$ )	NA
TS-TCH ( $q=8$ )	3.64 ( $\pm 0.1$ )	4.15 ( $\pm 0.07$ )	NA
TS-TCH ( $q=16$ )	6.16 ( $\pm 0.21$ )	6.9 ( $\pm 0.19$ )	NA
TS-TCH ( $q=32$ )	9.47 ( $\pm 0.47$ )	10.2 ( $\pm 0.4$ )	NA
$q$ EHVI-PM ( $q=1$ )	8.28 ( $\pm 0.22$ )	8.71 ( $\pm 0.04$ )	16.73 ( $\pm 0.1$ )
$q$ EHVI-PM ( $q=8$ )	115.8 ( $\pm 2.99$ )	OOM	133.39 ( $\pm 1.41$ )
$q$ EHVI ( $q=1$ )	4.67 ( $\pm 0.1$ )	9.63 ( $\pm 0.05$ )	5.69 ( $\pm 0.11$ )
$q$ EHVI ( $q=8$ )	104.48 ( $\pm 1.34$ )	OOM	68.95 ( $\pm 2.57$ )
$q$ NEHVI ( $q=1$ )	7.95 ( $\pm 0.1$ )	82.66 ( $\pm 0.63$ )	20.47 ( $\pm 0.12$ )
$q$ NEHVI ( $q=8$ )	67.28 ( $\pm 1.87$ )	683.06 ( $\pm 13.82$ )	168.04 ( $\pm 1.85$ )
$q$ NEHVI ( $q=16$ )	145.66 ( $\pm 4.45$ )	1289.4 ( $\pm 36.81$ )	362.15 ( $\pm 9.08$ )
$q$ NEHVI ( $q=32$ )	247.92 ( $\pm 11.93$ )	2480.41 ( $\pm 102.38$ )	654.66 ( $\pm 23.48$ )
$q$ NPAREGO ( $q=1$ )	4.86 ( $\pm 0.1$ )	3.25 ( $\pm 0.06$ )	6.17 ( $\pm 0.07$ )
$q$ NPAREGO ( $q=8$ )	48.62 ( $\pm 1.18$ )	30.65 ( $\pm 0.92$ )	38.66 ( $\pm 0.95$ )
$q$ NPAREGO ( $q=16$ )	122.09 ( $\pm 3.5$ )	81.04 ( $\pm 3.44$ )	84.27 ( $\pm 3.04$ )
$q$ NPAREGO ( $q=32$ )	275.41 ( $\pm 8.29$ )	219.98 ( $\pm 9.75$ )	199.6 ( $\pm 9.68$ )
$q$ PAREGO ( $q=1$ )	3.31 ( $\pm 0.07$ )	3.03 ( $\pm 0.06$ )	2.83 ( $\pm 0.08$ )
$q$ PAREGO ( $q=8$ )	33.84 ( $\pm 1.76$ )	22.0 ( $\pm 0.88$ )	20.28 ( $\pm 1.18$ )
$q$ PAREGO ( $q=16$ )	77.25 ( $\pm 3.9$ )	56.09 ( $\pm 3.09$ )	50.06 ( $\pm 3.84$ )
$q$ PAREGO ( $q=32$ )	217.55 ( $\pm 19.15$ )	139.25 ( $\pm 9.41$ )	135.39 ( $\pm 13.04$ )

Table 4. Acquisition function optimization wall time (including box decompositions) in seconds on a CPU (2x Intel Xeon E5-2680 v4 @ 2.40GHz) and a Tesla V100 SXM2 GPU (16GB RAM). The mean and two standard errors are reported.



(a) Sequential Optimization performance on additional benchmark problems.

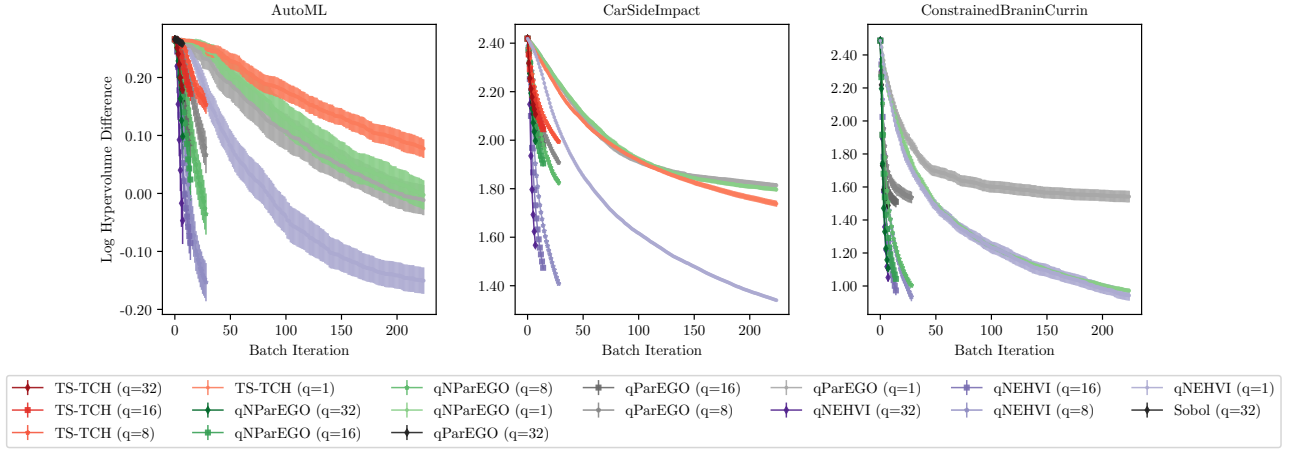
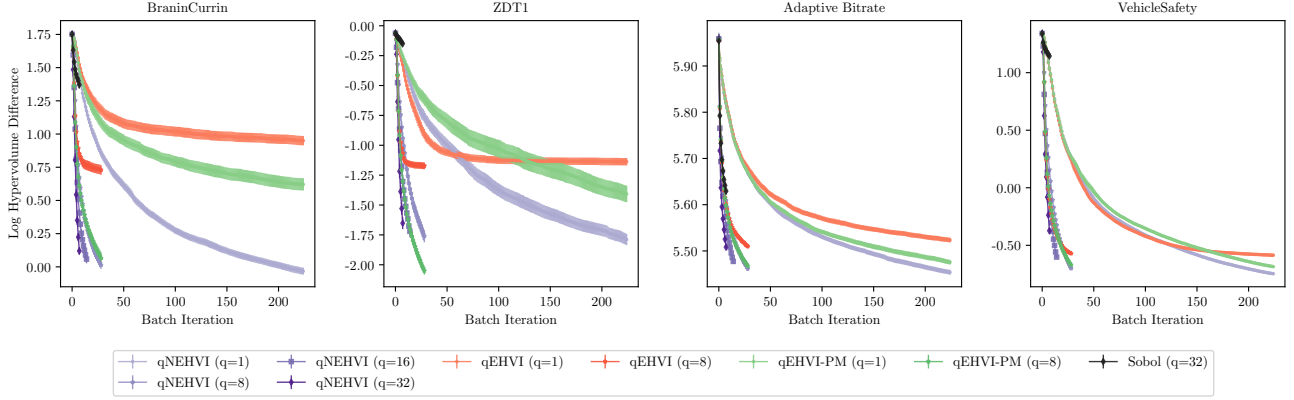
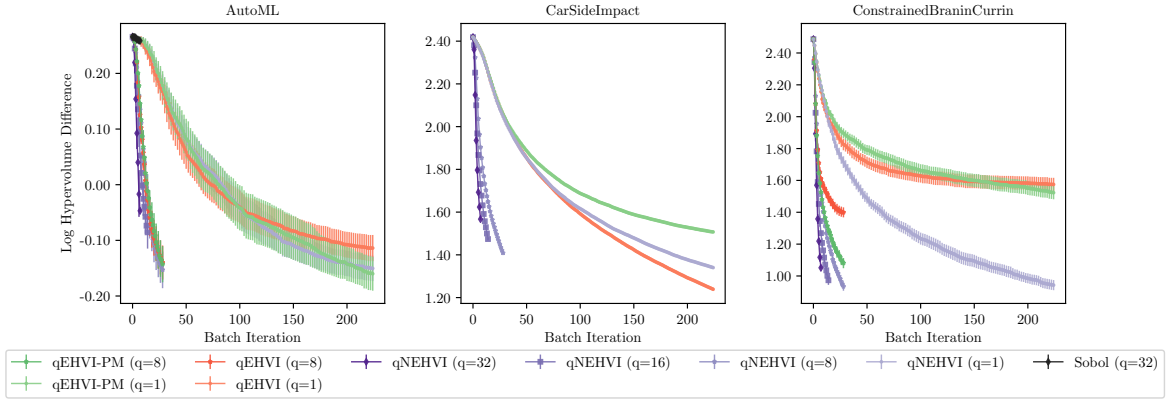

 (b) Parallel Optimization performance for various  $q$ .

Figure 6. Additional measures of optimization performance on additional problems.





(a)



(b)

Figure 7. Optimization performance of  $q$ NEHVI under various batch sizes  $q$  vs  $q$ EHVI(-PM). Note that using the IEP,  $q$ EHVI(-PM) cannot scale beyond  $q = 8$  because of the exponential time and space complexity (running it on a GPU runs out of memory and running it on a CPU results in unreasonably slow wall times).

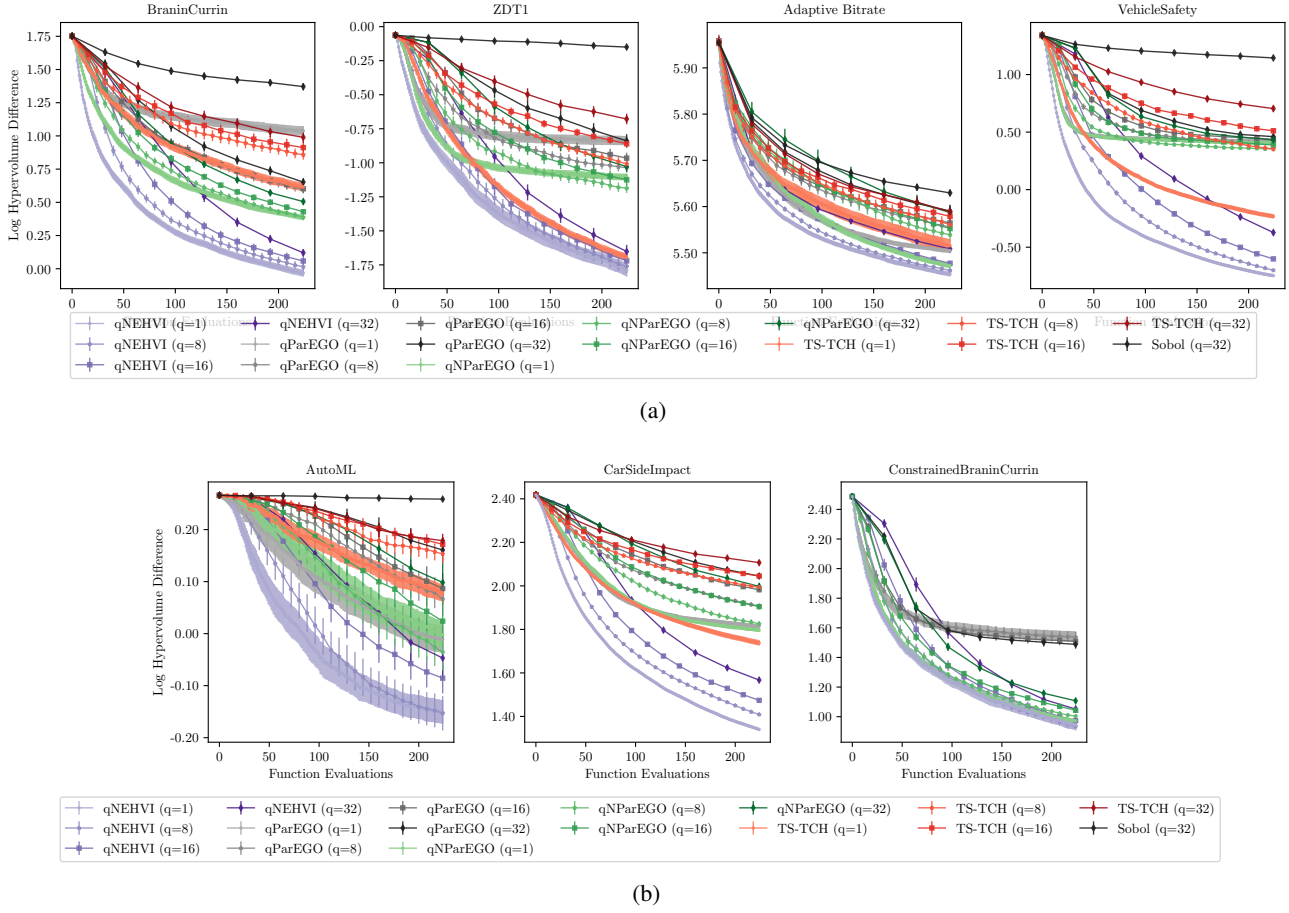
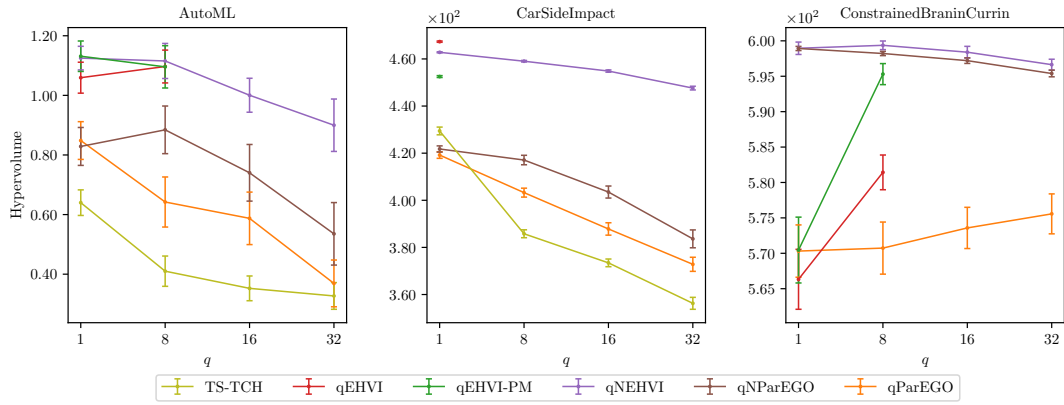


Figure 8. Anytime optimization performance of batch acquisition functions using various  $q$  over the number of function evaluations. To improve readability, we omit  $q$ EHVI(-PM) in this figure because the IEP cannot scale beyond  $q = 8$  because of the exponential time and space complexity (running it on a GPU runs out of memory and running it on a CPU results in unreasonably slow wall times).



## H. Noisy Outcome Constraints

While the focus of this work is on developing a scalable parallel hypervolume-based acquisition function for noisy settings, our MC-based approach naturally lends itself to support for constraints.

### H.1. Derivation of Constrained NEHVI

The NEHVI formulation in (3) can be extended to handle noisy observations of outcome constraints. We consider the scenario where we receive noisy observations of  $M$  objectives  $\mathbf{f}(\mathbf{x}) \in \mathbb{R}^M$  and  $V$  constraints  $\mathbf{c}^{(v)} \in \mathbb{R}^V$ , all of which are assumed to be “black-box”:  $\mathcal{D}_n = \{\mathbf{x}_i, \mathbf{y}_i, \mathbf{b}_i\}_{i=1}^n$  where  $\begin{bmatrix} \mathbf{y}_i \\ \mathbf{b}_i \end{bmatrix} \sim \mathcal{N}\left(\begin{bmatrix} \mathbf{f}(\mathbf{x}_i) \\ \mathbf{c}(\mathbf{x}_i) \end{bmatrix}, \Sigma_i\right)$ ,  $\Sigma_i \in \mathbb{R}^{(M+V) \times (M+V)}$ . We assume, without loss of generality, that  $\mathbf{c}^{(v)}$  is feasible iff  $c^{(v)} \geq 0$ . In the constrained optimization setting, we aim to identify the a finite approximate feasible Pareto set

$$\mathcal{P}_{\text{feas}} = \{\mathbf{f}(\mathbf{x}) \mid \mathbf{x} \in X_n, \mathbf{c}(\mathbf{x}) \geq \mathbf{0}, \nexists \mathbf{x}' : \mathbf{c}(\mathbf{x}') \geq \mathbf{0} \text{ s.t. } \mathbf{f}(\mathbf{x}') \succ \mathbf{f}(\mathbf{x})\}$$

of the true feasible Pareto set

$$\mathcal{P}_{\text{feas}}^* = \{\mathbf{f}(\mathbf{x}) \text{ s.t. } \mathbf{c}(\mathbf{x}) \geq \mathbf{0}, \nexists \mathbf{x}' : \mathbf{c}(\mathbf{x}') \geq \mathbf{0} \text{ s.t. } \mathbf{f}(\mathbf{x}') \succ \mathbf{f}(\mathbf{x})\}.$$

The natural improvement measure in the constrained setting is *feasible* HVI, which we define for a single candidate point  $\mathbf{x}$  as

$$\text{HVI}_c(\mathbf{f}(\mathbf{x}), \mathbf{c}(\mathbf{x}) \mid \mathcal{P}_{\text{feas}}) := \text{HVI}[\mathbf{f}(\mathbf{x}) \mid \mathcal{P}_{\text{feas}}] \cdot \mathbb{1}[\mathbf{c}(\mathbf{x}) \geq \mathbf{0}].$$

Taking the expectation over  $\text{HVI}_c$  gives the constrained expected hypervolume improvement:

$$\alpha_{\text{EHVI}_c}(\mathbf{x}) = \int \text{HVI}_c(\mathbf{f}(\mathbf{x}), \mathbf{c}(\mathbf{x}) \mid \mathcal{P}_{\text{feas}}) p(\mathbf{f}, \mathbf{c} \mid \mathcal{D}) d\mathbf{f} d\mathbf{c} \quad (22)$$

For brevity, we define  $\mathcal{C}_n = \mathbf{c}(X_n)$ . The *noisy expected hypervolume improvement* is then defined as:

$$\alpha_{\text{NEHVI}_c}(\mathbf{x}) = \int \alpha_{\text{EHVI}_c}(\mathbf{x} \mid \mathcal{P}_{\text{feas}}) p(\mathcal{F}_n, \mathcal{C}_n \mid \mathcal{D}_n) d\mathcal{F}_n d\mathcal{C}_n. \quad (23)$$

Performing feasibility-weighting on the sample-level allows us to include such auxiliary outcome constraints into the full Monte Carlo formulation given in (5) in a straightforward way:

$$\hat{\alpha}_{\text{NEHVI}_c}(\mathbf{x}) = \frac{1}{N} \sum_{t=1}^N \sum_{k=1}^{K_t} \left[ \prod_{m=1}^M [z_{k,t}^{(m)} - l_{k,t}^{(m)}]_+ \prod_{v=1}^V \mathbb{1}[c_t^{(v)}(\mathbf{x}) \geq 0] \right]$$

where  $z_{k,t}^{(m)} := \min[u_{k,t}^{(m)}, \tilde{f}_t^{(m)}(\mathbf{x})]$  and  $l_{k,t}^{(m)}, u_{k,t}^{(m)}$  are the  $m^{\text{th}}$  dimension of the lower and upper vertices of the rectangle  $S_{k,t}$  in the non-dominated partitioning  $\{S_{1,t}, \dots, S_{K_t,t}\}$  under the feasible sampled Pareto frontier

$$\mathcal{P}_{\text{feas},t} = \mathcal{P}_{\text{feas}} = \{\tilde{\mathbf{f}}_t(\mathbf{x}) \mid \mathbf{x} \in X_n, \tilde{\mathbf{c}}_t(\mathbf{x}) \geq \mathbf{0}, \nexists \mathbf{x}' : \tilde{\mathbf{c}}_t(\mathbf{x}') \geq \mathbf{0} \text{ s.t. } \tilde{\mathbf{f}}_t(\mathbf{x}') \succ \tilde{\mathbf{f}}_t(\mathbf{x})\}.$$

In this formulation, the  $\prod_{v=1}^V \mathbb{1}[c_t^{(v)}(\mathbf{x}) \geq 0]$  indicates feasibility of the  $t$ -th sample.

To permit gradient-based optimization via exact sample-path gradients, we replace the indicator function (which is non-differentiable) with a differentiable sigmoid approximation with a temperature parameter  $\tau$ , which becomes exact as  $\tau \rightarrow \infty$ :

$$\mathbb{1}[c^{(v)}(\mathbf{x}) \geq 0] \approx s(c^{(v)}(\mathbf{x}); \tau) := \frac{1}{1 + \exp(-c^{(v)}(\mathbf{x})/\tau)} \quad (24)$$

Hence,

$$\hat{\alpha}_{\text{NEHVI}_c}(\mathbf{x}) \approx \frac{1}{N} \sum_{t=1}^N \sum_{k=1}^{K_t} \left[ \prod_{m=1}^M [z_{k,t}^{(m)} - l_{k,t}^{(m)}]_+ \prod_{v=1}^V s(c_t^{(v)}(\mathbf{x}), \tau) \right]$$

## H.2. Derivation of Parallel, Constrained NEHVI

The constrained NEHVI can be extended to the parallel setting in a straightforward fashion. The joint constrained hypervolume improvement of a set of points  $\{\mathbf{x}_i\}_{i=1}^q$  is given by

$$\text{HVI}_c(\{\mathbf{f}(\mathbf{x}_i), \mathbf{c}(\mathbf{x}_i)\}_{i=1}^q) = \sum_{k=1}^K \sum_{j=1}^q \sum_{\mathbf{x}_j \in \mathcal{X}_j} (-1)^{j+1} \left[ \left( \prod_{m=1}^M [\mathbf{z}_{k, \mathbf{x}_j}^{(m)} - l_k^{(m)}]_+ \right) \prod_{\mathbf{x}' \in \mathcal{X}_j} \prod_{v=1}^V \mathbb{1}[c^{(v)}(\mathbf{x}') \geq 0] \right].$$

and the constrained  $q\text{EHVI}$  is (Daulton et al., 2020):

$$\alpha_{q\text{EHVI}_c}(\mathcal{X}_{\text{cand}} | \mathcal{P}_{\text{feas}}) = \int \text{HVI}_c(\mathbf{f}(\mathcal{X}_{\text{cand}}), \mathbf{c}(\mathcal{X}_{\text{cand}}) | \mathcal{P}_{\text{feas}}) p(\mathbf{f}, \mathbf{c} | \mathcal{D}_n) d\mathbf{f} d\mathbf{c}$$

Hence, the constrained  $q\text{NEHVI}$  is given by:

$$\begin{aligned} \alpha_{q\text{NEHVI}_c}(\mathcal{X}_{\text{cand}}) &= \int \alpha_{q\text{EHVI}_c}(\mathcal{X}_{\text{cand}} | \mathcal{P}_{\text{feas}}) p(\mathcal{F}_n, \mathcal{C}_n | \mathcal{D}_n) d\mathcal{F}_n d\mathcal{C}_n \\ &= \int \text{HVI}_c(\mathbf{f}(\mathcal{X}_{\text{cand}}), \mathbf{c}(\mathcal{X}_{\text{cand}}) | \mathcal{P}_{\text{feas}}) p(\mathcal{F}_n, \mathcal{C}_n | \mathcal{D}_n) d\mathcal{F}_n d\mathcal{C}_n \end{aligned} \quad (25)$$

Using MC integration for the integral in (25), we have

$$\hat{\alpha}_{q\text{NEHVI}_c}(\mathcal{X}_{\text{cand}}) = \frac{1}{N} \sum_{t=1}^N \text{HVI}_c(\tilde{\mathbf{f}}_t(\mathcal{X}_{\text{cand}}), \tilde{\mathbf{c}}_t(\mathcal{X}_{\text{cand}}) | \mathcal{P}_{\text{feas}, t}). \quad (26)$$

Under the CBD formulation, the constrained  $q\text{NEHVI}$  is given by

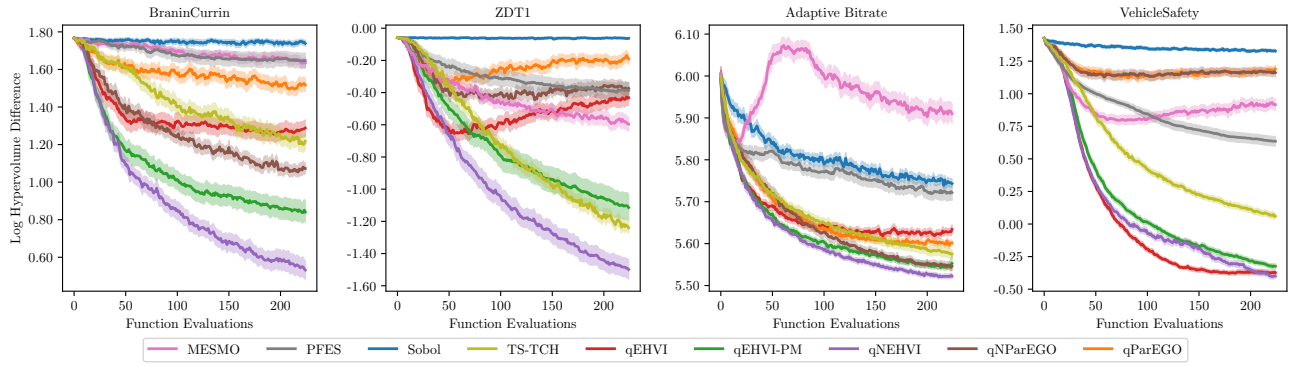
$$\begin{aligned} \hat{\alpha}_{q\text{NEHVI}}(\{\mathbf{x}_1, \dots, \mathbf{x}_i\}) &= \frac{1}{N} \sum_{t=1}^N \text{HVI}_c(\{\tilde{\mathbf{f}}_t(\mathbf{x}_j), \tilde{\mathbf{c}}_t(\mathbf{x}_j)\}_{j=1}^{i-1} | \mathcal{P}_{\text{feas}, t}) + \frac{1}{N} \sum_{t=1}^N \text{HVI}_c(\tilde{\mathbf{f}}_t(\mathbf{x}_i), \tilde{\mathbf{c}}_t(\mathbf{x}_i) | \mathcal{P}_{\text{feas}, t} \cup \{\tilde{\mathbf{f}}_t(\mathbf{x}_j), \tilde{\mathbf{c}}_t(\mathbf{x}_j)\}_{j=1}^{i-1}). \end{aligned} \quad (27)$$

As in (9), the first term is a constant when generating candidate  $i$  and the second term is the NEHVI of  $\mathbf{x}_i$ .

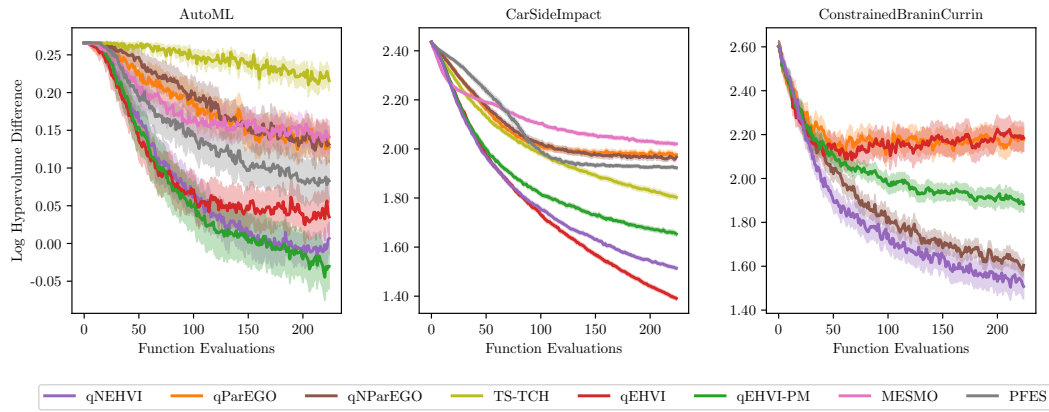
## I. Evaluating Methods on Noisy Benchmarks

Given noisy observations, we can no longer compute the true Pareto frontier over the in-sample points  $X_n$ . Moreover, the subset of Pareto optimal designs  $\mathcal{X}_n^* = \{\mathbf{x} \in X_n, \nexists \mathbf{x}' \in X_n \text{ s.t. } \mathbf{f}(\mathbf{x}') \succ \mathbf{f}(\mathbf{x})\}$  from the previously evaluated points may not be identified due to noise. For the previous results reported in this paper, we evaluate each method according to hypervolume dominated by the true unknown Pareto frontier of the noiseless objectives over the *in-sample* points. In practice, decision-makers would often select one of the in-sample points according to their preferences. If the decision maker only has noisy observations, selecting an in-sample point may be preferable to evaluating a new out-of-sample point according to the model's beliefs. An alternative evaluation method would be use the model's posterior mean to identify what it believes is the Pareto optimal set of in-sample designs. The hypervolume dominated by the true Pareto frontier of noiseless objectives over that set of selected designs could be computed and used for comparing the performance of different methods. Results using this procedure are shown in Figure 10. The quality of the Pareto set depends on the model fit. Several methods have worse performance over time (e.g.  $q\text{EHVI}$  and  $q\text{PAREGO}$  on the ZDT1 problem), likely due to the collection of outlier observations that degrade the model fit. Nevertheless,  $q\text{NEHVI}$  consistently has the strongest performance.

An alternative to the *in-sample* evaluation techniques described above would be to use the model to identify the Pareto frontier across the entire search space (in-sample or *out-of-sample*). For example, Hernández-Lobato et al. (2015) used NSGA-II to optimize the model's posterior mean and identify the model estimated Pareto frontier. For benchmarking purposes on expensive-to-evaluate functions (e.g. in AutoML or ABR), this is unreasonably expensive. Moreover, such a method is less appealing in practice because a decision-maker would have to select out-of-sample points according to the posterior mean and then evaluate a set of preferred designs on the noisy objective to verify that the model predictions are fairly accurate at those out-of-sample designs. Therefore, in this work we evaluate methods based on the in-sample designs.



(a)



(b)

Figure 10. Sequential optimization performance using based on the model-identified Pareto set across in-sample points.